



The 100-ka and rapid sea level changes recorded by prograding shelf sand bodies in the Gulf of Lions (western Mediterranean Sea)

M. A. Bassetti and S. Berné

Institut de Modélisation et d'Analyse en Géo-Environnement et Santé, Université de Perpignan, 52 avenue Paul Alduy, F-66860 Perpignan, France

Géosciences Marines, Institut Français de Recherche pour l'Exploitation de la Mer, BP70, F-29280 Plouzané, France (maria-angela.bassetti@univ-perp.fr)

G. Jouet

Géosciences Marines, Institut Français de Recherche pour l'Exploitation de la Mer, BP70, F-29280 Plouzané, France

M. Taviani

Istituto di Scienze Marine, CNR, via Gobetti 101, I-40129 Bologna, Italy

B. Dennielou

Géosciences Marines, Institut Français de Recherche pour l'Exploitation de la Mer, BP70, F-29280 Plouzané, France

J.-A. Flores

Facultad de Ciencias, Universidad de Salamanca, Plaza Merced s/n, E-37008 Salamanca, Spain

A. Gaillot

Altran Quest, Technopole Brest Iroise, CS 23866, F-29238 Brest, CEDEX 3, France

R. Gelfort

Institut für Geowissenschaftliche Gemeinschaftsaufgaben, Stilleweg 2, D-30655 Hannover, Germany

S. Lafuerza

GRC Geociències Marines, Departament d'Estratigrafia i Paleontologia i Geociències Marines, Universitat de Barcelona, Martí i Franquès s/n, E-08028 Barcelona, Spain

N. Sultan

Géosciences Marines, Institut Français de Recherche pour l'Exploitation de la Mer, BP70, F-29280 Plouzané, France

[1] Thick forced regressive units on the wide continental shelf of the Gulf of Lions (western Mediterranean) recorded the composite effect of sea level changes during the Quaternary. They are mostly composed of coastal siliciclastic and bioclastic wedges showing clinof orm geometry. These deposits have been intensively explored through high-resolution seismic investigations, but only recently it was possible to ground truth seismic interpretations, based on a long (100 m) borehole that crossed the succession and recovered a large part of the mainly sandy deposits (~84% recovery). A multiproxy analysis of the sedimentary succession shows that (1) the stratal architecture of the shelf margin is defined by major bounding surfaces that are polygenic erosion surfaces associated with coarse-grained material incorporating abundant and diverse shells, including cold-water fauna (presently absent from the

Mediterranean Sea). Between each surface, coarsening upward units with steep (up to 5°) foresets are made of massive (more than 20 m thick) sands with possible swaley and hummocky cross-stratification, passing seaward to sands with muddy intervals and, further offshore, alternating highly bioturbated sands and silts. Each prograding wedge corresponds to a forced-regressive shoreface (or delta front/prodelta), deposited during the overall sea level falls occurring at (relatively slow) interglacial/glacial transition and therefore represents the record of 100 ka cyclicality. Higher-frequency Milankovitch cyclicities are also probably represented by distinct shoreface/delta front wedges; (2) detailed examination of the architecture and chronostratigraphy of the most recent sequence shows that minor bounding surfaces, corresponding to abrupt shallowing of sedimentary facies, separate downward stepping parasequences within the last 100 ka sequence. These events are in phase with millennial-scale glacial climatic and sea level variability, the downward shift surfaces corresponding to the falls during the coldest stadials. These deposits provide a comprehensive and well-constrained Pleistocene analog to the numerous shoreface deposits attributed to falling-stage systems tracts recognized in ancient stratigraphic records, studied at the outcrop scale.

Components: 12,008 words, 13 figures.

Keywords: shoreface; quaternary; Mediterranean; paleoclimate.

Index Terms: 1861 Hydrology: Sedimentation (4863); 1641 Global Change: Sea level change (1222, 1225, 4556).

Received 12 October 2007; **Revised** 29 August 2008; **Accepted** 10 September 2008; **Published** 13 November 2008.

Bassetti, M. A., S. Berné, G. Jouet, M. Taviani, B. Dennielou, J.-A. Flores, A. Gaillot, R. Gelfort, S. Lafuerza, and N. Sultan (2008), The 100-ka and rapid sea level changes recorded by prograding shelf sand bodies in the Gulf of Lions (western Mediterranean Sea), *Geochem. Geophys. Geosyst.*, 9, Q11R05, doi:10.1029/2007GC001854.

Theme: Interactions Between High-Frequency Climate Changes and Deltaic Margin Architecture

Guest Editors: S. Berné, J. Syvitski, and F. Trincardi

1. Introduction

[2] Prograding beach-shoreface deposits are a common component of the stratigraphic record [Walker and Plint, 1992]. They correspond to one of the key “facies models” utilized by sedimentologists studying the stratigraphic record, and the analysis of their evolution through time is at the origin of most sequence-stratigraphic paradigms [Posamentier *et al.*, 1992]. Beach-shoreface deposits are very sensitive to base-level changes, thus they have been also utilized, under certain conditions, as “dipsticks” for sea level changes [Rabineau *et al.*, 2006]. In addition, because of their high content of well-sorted sand, they also represent potential reservoirs for hydrocarbons. However, the shallow marine processes that are recorded in detail within shoreface-foreshore-shelf parasequences are barely known. This is mostly due to the lack of lithological data on Quaternary shoreface deposits, which are mainly known through high-resolution seismic investigations or from interpretation of outcrops examples of ancient shoreface deposits. The term “shoreface” is used here in the sense of van Wagoner *et al.* [1990], i.e., sedi-

ments deposited between the foreshore and the storm wave base. In a wave-dominated deltaic setting, it corresponds to the delta front and prodelta domains, and it is generally difficult, in the stratigraphic record, to make the distinction between both settings, especially when longshore drift modifies the geometry of sand bodies [Bhattacharya and Giosan, 2003].

[3] The Gulf of Lions, in the NW Mediterranean Sea has been the subject of intense high-resolution seismic investigations during the last 10 years [Berné *et al.*, 2004]. Because of high sediment supply and rapid subsidence it offers an exceptional record of shelf/slope sequences linked to glacioeustatic sea level changes during the last 500 ka. However, attempts to core the sand bodies deposits that constitute one of the key component of the shelf/slope succession was largely unsuccessful, due to the presence of coarse shell lags making piston and vibra-coring operations very difficult. The maximum recovery using these conventional techniques were cores about 2.5 m long [Aloisi, 1986; Bassetti *et al.*, 2006; Berné *et al.*, 1998]. For similar reasons, Ocean Drilling Program (ODP) leg

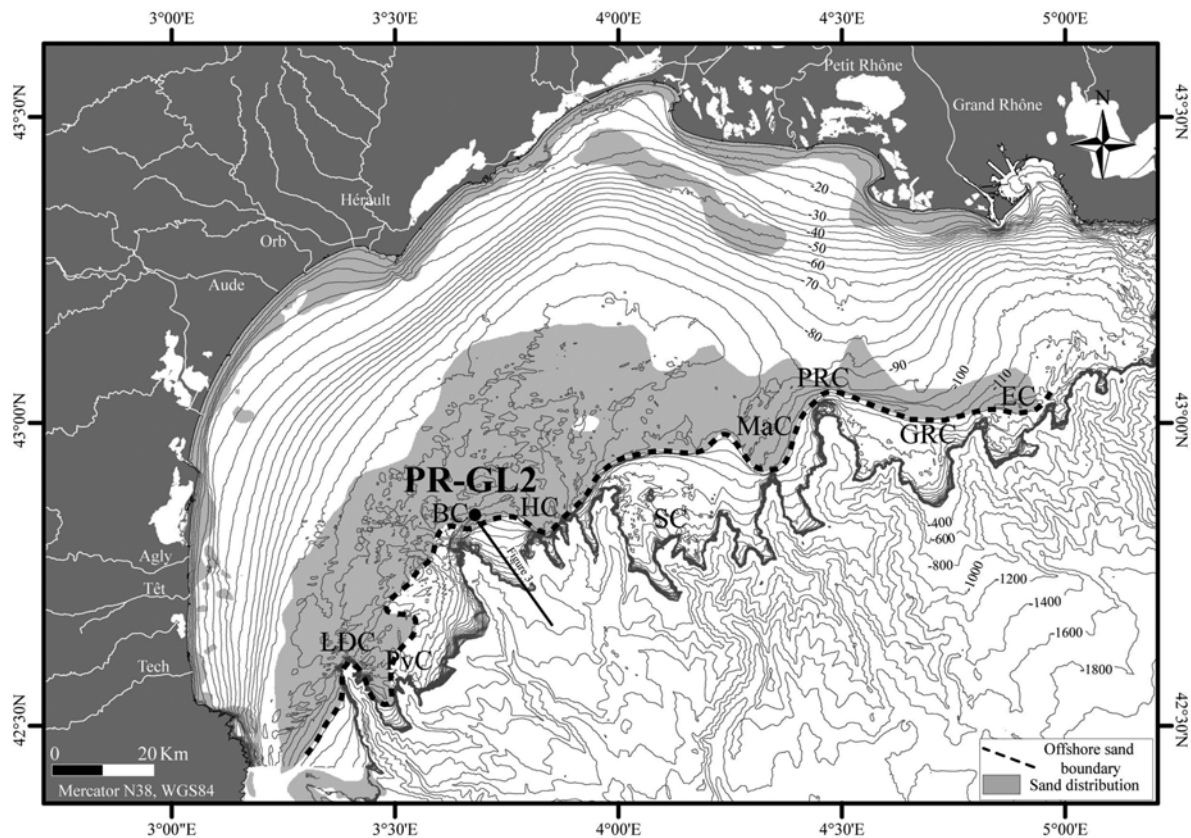


Figure 1. General bathymetry of the Gulf of Lions. The gray pattern corresponds to the sand distribution on continental shelf. The dotted line marks the seaward termination of glacial sandy shorefaces.

174A on the New Jersey continental shelf encountered great difficulties recovering, with “advanced piston coring,” the sandy successions that constitute most of Quaternary deposits on this margin [Austin *et al.*, 1998]. Similarly, attempts to core a sand ridge in the North Sea experienced major difficulties, with an overall recovery less than 16% [Davis and Balson, 1992]. The most comprehensive investigation of sandy clinoforms was conducted by a consortium of oil companies, which successfully drilled shelf-edge deltas of the Mississippi margin [Winn *et al.*, 1995]. However, the borehole described by these authors is located beyond the shelf edge, and the authors do not provide description of sedimentary facies within the clinoform units.

[4] In June–July 2004, a drilling operation was funded by the European Community in order to investigate the Adriatic and the Gulf of Lions deltaic margins (Profiles Across Mediterranean Sedimentary Systems (PROMESS 1)). Two sites were drilled in the Gulf of Lions: PRGL1-4 (300 m long), located at the interfluvial of Bourcart and Hérault canyons at a water depth of 298 m, and PRGL2-2 (100 m long, 103 m water depth),

through the seaward termination of a preserved last glacial shoreline (Figure 1). In particular, PRGL2-2 drilled through sedimentary discontinuities related to submarine and/or subaerial erosion that can be tied to correlative conformities toward the slope. The borehole provided valuable information on seismic and sedimentary facies, as well as physical and geotechnical properties.

[5] Interpretations of the prograding sediment wedges that were drilled during the cruise at site PRGL2-2 are here provided, since the drilling operations were successfully terminated with the satisfactory core recovery of 84%, despite the presence of thick sandy intervals. The correspondence between sedimentary and seismic facies is here demonstrated, thanks to the newly acquired sedimentological data that permit detailed characterization the seismic response to lithological changes. For intervals with no recovery, lithologies were predicted from Cone Penetration Test [Lafuerza *et al.*, 2008].

[6] The major objectives of our study are to describe the sedimentary facies of clinothem units and interpret their depositional environment and to



understand how the different facies and sequences record the changing sea level and how important surfaces can be recognized from subsurface and sedimentological data.

2. Regional Setting

[7] The Gulf of Lions is a passive, prograding, and subsiding margin, located in the northwestern sector of the Mediterranean Sea bounded, to the west and east, by Pyrenean and Alpine orogenic belts, respectively (see the synthesis by *Berné and Gorini* [2005]). It comprises a wide (about 70 km) shelf and a continental slope that is incised by numerous canyons descending to the abyssal area of the Algero-Balearic Basin. Because of high sediment supply (mainly from the Alps through the Rhône River) and very limited tectonic activity, the Gulf of Lions is a favorable environment for studying the deposition and preservation of sequences controlled by glacioeustasy.

[8] During the last ~ 500 ka, sea level oscillated between its present position and about 120 m below the present sea level. Because the shelf edge is located between 105 and 165 m water depth, a large portion of the continental shelf was exposed during glacial periods. As a result, the stratigraphic record displays major erosional surfaces resulting from subaerial and shallow marine erosion during sea level falls, lowstands, and sea level rises.

[9] The cyclically stacked Plio-Quaternary sequences have been object of seismic investigations over the last 30 years by several authors who proposed a number of conceptual and/or numerical stratigraphic models [*Aloisi*, 1986; *Berné et al.*, 1998; 2004; *Lofi et al.*, 2003; *Monaco*, 1971; *Rabineau et al.*, 2005; *Tesson et al.*, 1990; 2000]. A review of these investigations is given by *Rabineau et al.* [2005]. Most of the middle and outer continental shelf consists of prograding wedges that display internal reflections showing alternating low angle ($<1^\circ$) and high angle ($>4^\circ$) clinoforms. On the basis of shallow cores and stratigraphic modeling, this elementary “motif” was interpreted as the result of alternating deposition of high energy (sandy upper shorefaces/delta fronts) and low energy (muddy lower shorefaces or “offshore” deposits) during late Quaternary sea level changes. The large (>100 km) lateral extent of these sand bodies suggest a global (sea level) control on their deposition. However, the nature of the prograding shorefaces remained controversial; some authors interpreted them as the product of

deposition during the falling stage of sea level [*Aloisi*, 1986; *Berné et al.*, 1998; *Rabineau et al.*, 2005], whereas others proposed that they could correspond to transgressive parasequences (in the sense of *van Wagoner et al.* [1990]) formed during the early stages of sea level rises [*Tesson et al.*, 2000]. Also, the formation timing of these deposits remained elusive, with some authors interpreting the major bounding surfaces separating each prograding unit as sequence boundaries linked to the 100 ka glacial/interglacial cycles [*Aloisi*, 1986; *Lobo et al.*, 2005; *Rabineau*, 2001], whereas others ascribed them to higher-order (20 ka) cyclicities [*Tesson et al.*, 1993, 2000].

3. Methods

[10] The data were collected on board SRV *Bavenit* of the Russian company Amige, operated by Fugro. In order to evaluate sediment types to be cored, and for geotechnical characterization, we first performed a continuous cone penetration test unified (CPTU) at site PRGL2-1, distant a few m from the PRGL2-2 site where continuous coring was carried out. The test was made with a static penetrometer measuring (1) cone resistance (kPa); (2) sleeve friction (kPa); and (3) pore pressure acting on the cone (kPa). The CPTU equipment and the procedures adopted during the cruise operations are in accordance with the International Reference Test Procedure published by the *Society of Soil Mechanisms and Geotechnical Engineering (ISSMGE)* [1999]. Estimation of sediment types based on geotechnical properties was done using the method of soil classification established after *Ramsey* [2002].

[11] An important application of CPTU measurements is the prediction of the stratigraphy and lithology of buried sediments. Thanks to the combination of three CPTU measurements (cone resistance, lateral friction, pore pressure [*Ramsey*, 2002]) it is possible to define the soil type based on a soil classification chart (see details in the work of *Lafuerza et al.* [2008]). It relies on a large CPTU database adapted and improved by different authors to diagrams of soil classification [*Ramsey*, 2002; *Robertson*, 1990].

[12] All geotechnical data were combined for soil characterization, considering that the pore pressure (u_2) is mainly related to the permeability of sediments, whereas the resistance to cone penetration (qt) and the lateral friction (fs) can be directly correlated to a particular lithology.

[13] Core sections, from 0.80 to 1.5 m in length, were recovered using a suite of FUGRO corers, including a piston corer, a “WIP” corer, and a FUGRO corer. Overall, about 50% of the drilled section consisted of sand, making core recovery difficult. However, within very sandy intervals, the strategy consisted to core down to the maximum of penetration, then, when core recovery was less than 50 cm, to drill only 50 cm in order to minimize the gaps. This time-consuming operation allowed overall recovery of 84%.

[14] Physical properties of collected cores were measured on board using a GEOTEK MultiSensor Core Logger (MSCL), by means of (1) gamma ray density; (2) *P* wave velocity; and (3) magnetic susceptibility. Magnetic susceptibility was measured a second time in the laboratory on split cores. To link lithological, seismic, and geotechnical data, a time-depth conversion was constructed using *P* wave velocities from MSCL. From this calculation, all logs were converted into a timescale (ms; two way travel time (TWTT)). In addition, velocities of fine-grained intervals were measured using a pair of transducers oriented along the core axis. The very good match between major lithological changes and boundaries of seismic units demonstrates the validity of the method.

[15] All cores were visually described, and X-ray images were realized for the most significant sections. The X-ray radiography was particularly useful for enhancing subtle sedimentary structures not easily identified on freshly cut core surfaces.

[16] Measurements of carbonate content (Bernard calcimeter, precision $\pm 2\%$) and grain size analyses with a laser microgranulometer (Coulter counter LS130; size range 0.4 μm to 1 mm) were made on the total sediment fraction on samples collected every 20 cm (with the exception of gravel beds).

[17] In order to establish a biostratigraphic control, the cores were analyzed onboard for calcareous nannoplankton (E. Colmenero and J. Gravalosa, personal communication, 2004), additional samples being analyzed after core splitting in the laboratory.

[18] The chronostratigraphy of the youngest sequence is based on AMS ^{14}C dating of biogenic carbonates (mainly Foraminifera). In addition, attempts were made on a few samples to date total organic carbon or wood fragments. Approximately 10 mg of biogenic carbonate was handpicked under the binocular microscope and AMS ^{14}C dates were obtained by the Poznan Radiocarbon Laboratory of the Adam Mickiewicz University (Poland). All

ages reported here are given in calibrated ages. For ages between 0 and 21,880 ^{14}C BP calendar (i.e., calibrated) ages were calculated using correction tables [Stuiver and Reimer, 1993] and by mean of Calib 5.0.2 software (<http://calib.qub.ac.uk/calib/>). For the marine material, the Marine04 calibration curve [Hughen et al., 2004; Reimer et al., 2004] was used with no deviation from the mean global reservoir correction (-400 y). For continental material the Intcal04 calibration curve [Reimer et al., 2004] was used. For ages beyond 21,880 ^{14}C BP, the Glacial Polynomial [Bard et al., 1998] was used. Calendar ages are given with 1 sigma standard error.

[19] Beyond the radiocarbon dating resolution, chronostratigraphy was obtained by estimations of the abundance of biostratigraphically significant coccolith taxa, following the criteria of Raffi and Flores [1995].

[20] In addition to core data, spectral gamma ray measurements were performed in situ by means of wireline logging. Total gamma counts and potassium (^{40}K), thorium (^{232}Th), and uranium (^{238}U) fractions were recorded. Because open hole logging was deemed to be too risky in such unconsolidated marine sediments, logging took place within the drill string and bottom hole assembly (BHA). While this ensured a safe operation, gamma counts were severely diminished by the surrounding steel. From the BHA design, steel thicknesses were established and data corrected for using the ENCOR algorithm as developed by Hendriks [2003]. Spectral gamma ray results showed no major features but total gamma ray counts were utilized as clean sand versus clay indicator.

4. Results

4.1. Seismic Sequences and Surfaces

[21] The overall seismic stratigraphic organization of the shelf/upper slope is summarized in Figure 2. In the Gulf of Lions margin, prograding wedges, attributed to forced-regressive systems tracts [Hunt and Tucker, 1992] thicken seaward. These wedges are bounded by erosion surfaces that become correlative conformities on the upper continental slope, where they have been precisely dated. They form a hierarchy of bounding surfaces in the sense of Brookfield [1977].

[22] Major seismic surfaces are traceable throughout the Gulf of Lions and they correspond to 100 ka glacioeustatic cycles [Rabineau et al., 2005]. They

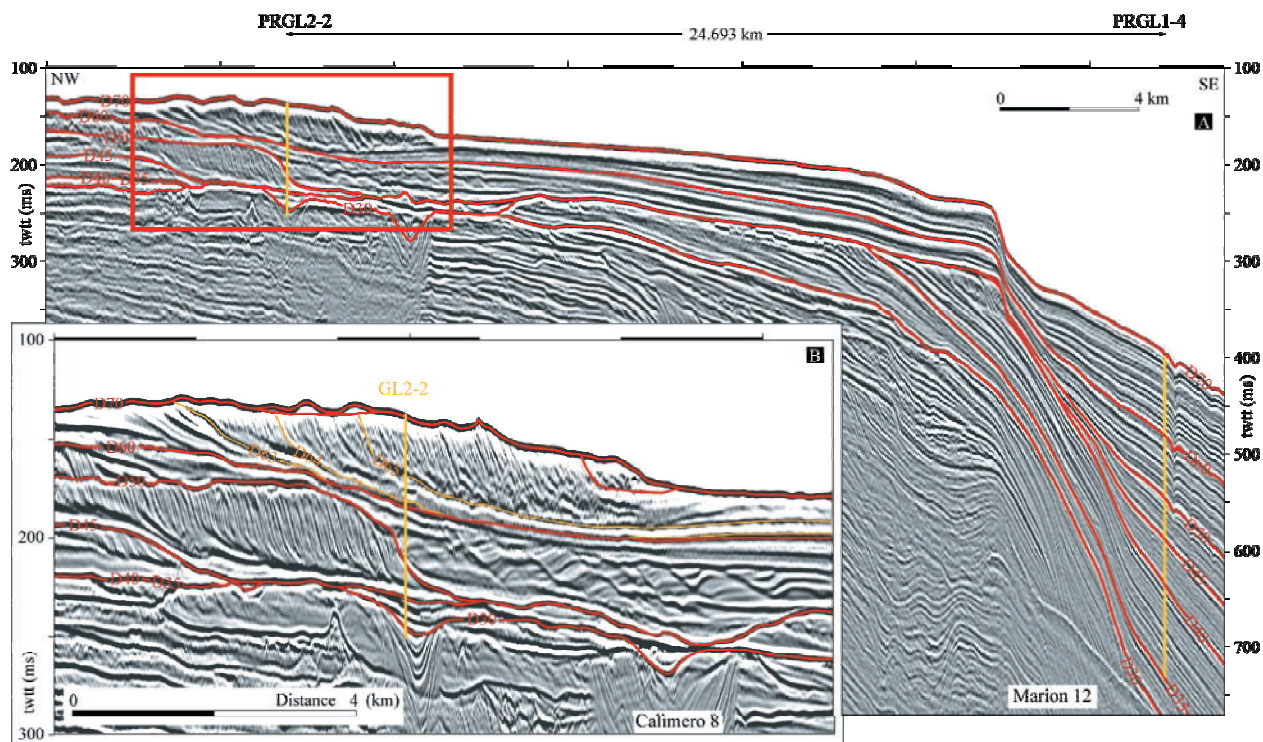


Figure 2. Multichannel, high-resolution seismic profiles at the drill site: (a) shelf-slope seismic line (Marion 12) showing depositional sequences bounded by discontinuities on the shelf that can be followed into correlative conformities on the slope (PRGL1–4 site); (b) close-up view at the position of PRGL2-2 (line Calimero 8).

bound major seismic units. Minor seismic surfaces have not been correlated at the regional scale [Jouet, 2007], but display an erosional geometry, or distinct changes in clinoform geometries, within major seismic units. These minor surfaces have been correlated to distinct and well-dated climatic/sea level events identified in long piston cores [Jouet et al., 2006] or in the PROMESS 1 drill sites.

[23] In the vicinity of PRGL2-2, seismic facies seen on multichannel and sparker profiles (Figure 3) are characterized by various clinoform geometries. From the top to the bottom of the borehole, six major seismic units are identified (see further details in the Auxiliary Material)¹:

[24] 1. Unit U150 is characterized by steep (up to 5°) clinoforms pinching out seaward and forming a ~48 ms (42 m) thick wedge interpreted as a forced regressive and lowstand shoreface [Rabineau et al., 2006]. Cemented sands (C.S. in Figure 3), interpreted as beach rocks by Berné et al. [1998] and Jouet et al. [2006] are exposed on the seafloor 1 km south of the drill site (Figure 3). Within U150,

several minor bounding surfaces identified on the Bourcart-Hérault interfluvium [Jouet et al., 2006] have been recognized here in this proximal depositional environment. At PRGL2-2 position, D63 is an erosion surface dated between 41 and 38 cal ka BP [Jouet et al., 2006]. D64 and D65 display more subtle changes, but these surfaces are traceable in a strike direction for over 15 km (D64) and across the entire shelf edge (D65) [Jouet, 2007]. These bottomsets form the downlap surface for high-angle clinoforms deposited subsequently (Figure 3). These minor bounding surfaces allow the identification, within U150, of four seismic subunits, labeled U147, U151a, U151b, U152 (Figure 3) [Jouet et al., 2006]. In addition, a subhorizontal minor bounding surface truncates the upper part of the clinoforms of U150. A large number of shallow cores and ultrahigh resolution seismic profiles have shown that it is a ravinement surface dated between 15 and 16 cal ka BP (at 99 m water depth) that formed during the last deglacial sea level rise [Bassetti et al., 2006]. Locally, this surface underlies elongated sand bodies (unit 155 of Figure 3), several kilometers long, some hundred meters wide, and 5–10 m thick, oriented NW–SE and interpreted as transgressive sand ridges [Bassetti et al., 2006].

¹Auxiliary materials are available in the HTML. doi:10.1029/2007GC001854.

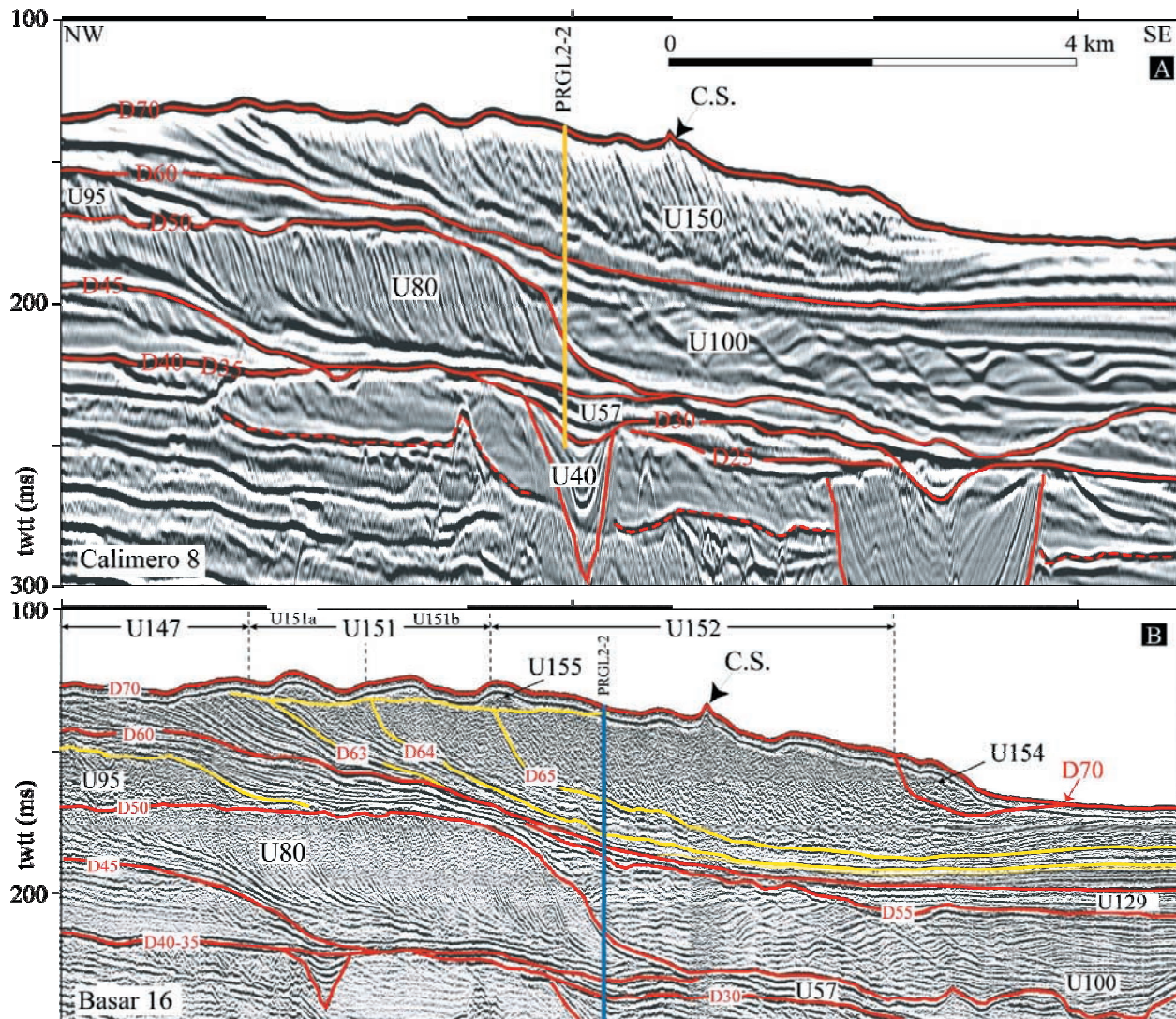


Figure 3. (a) High-resolution multichannel and (b) very high-resolution (sparker) seismic profiles showing the detail on the last sequence (bounded by D60 and D70 discontinuities). See position in Figures 1 and 2. Postglacial transgressive deposits (U155) lie above the clinostratified sequence. C.S. is cemented sand.

[25] 2. Unit U129 is a seaward thickening wedge made of very low-angle clinoforms (high-amplitude, parallel reflections). Its upper termination (D60) is an erosion surface (see left-hand side of Figure 3b) that seaward becomes a correlative conformity.

[26] 3. Unit U100 displays continuous, low-angle clinoforms shaped, seaward of unit 80, into wavy structures, that could be interpreted either as submarine retrogressive slides or, more likely, sediment waves (see the review by Lee *et al.* [2002]). These structures are asymmetrical with a steep side facing upslope, suggesting landward migration if they are sediment waves. In three dimensions, this

unit also displays three subunits [Rabineau *et al.*, 2005].

[27] 4. Unit U80 displays seismic facies similar to that of U151/152 at PRGL2-2 position, with clinoforms dipping at angles up to 5°, but the topsets are better preserved as in U151/152 and their sigmoid shape is clearly visible (Figure 3).

[28] Below these prisms, several major erosion bounding surfaces are observed at the position of PRGL2-2 (D45, D40, D35, and D30). D45-40-35 corresponds to three erosion surfaces, amalgamated on the shelf and that separate seaward (Figure 2). Hereafter, it will be named D45 (Figure 3). Between

these erosion surfaces, Unit U57 is a <5 m-thick seismic unit, difficult to correlate laterally. The bottom of the borehole reached seismic Unit U40 that corresponds to the infill of an axial incision (in the sense of *Baztan et al.* [2005]) cutting across a major buried canyon connected to the present Bourcart Canyon (Figure 1).

4.2. Lithology, Bio-, and Sedimentary Facies of Seismic Units

[29] PRGL2-2 offers a unique opportunity to verify the actual nature of sandy clinofolds that have been imaged all around the world but almost never sampled with satisfying recovery.

[30] At the core scale, 14 sedimentary units were identified on the basis of their sedimentary facies (Table S1, Auxiliary Material). They are bounded by five coarse-grained intervals, the positions of which perfectly correspond to the five major bounding surfaces (D70, D60, D50, D45, D30) previously described on seismic profiles (Figure 4). The detailed lithological description of the borehole is included in the Auxiliary Material, as well as the geotechnical properties (Figure 5) that were utilized to interpolate with good confidence the lithological information for nonrecovered intervals.

[31] 1. U152 is an overall coarsening upward sequence as defined on the basis of lithology, grain size, and gamma ray (sedimentary unit 1; Figures 4 and 6). This unit is topped by a coarse to medium sand interval, 1.90 m thick, with shell debris (D70). It displays laminated or cross-bedded well-sorted and homogeneous fine- to medium-grained sand, with scattered rounded pebbles. Thin (1–2 cm) mud interbeds occur within the lower part of this interval (Figure 7, sections 8A, 10A, 14A; Figure 9, image 1). Swaley cross-stratification [*Leckie and Walker*, 1982] or hummocky cross-stratification [*Harms et al.*, 1975] can be inferred at levels (Figure 7, section 14A) but these large-scale sedimentary structures are not easy to recognize at core scale.

[32] 2. U151 (sedimentary unit 2) is also a coarsening upward sequence consisting of mud-sand alternations with millimeter-thick sandy beds, laminated and intensely burrowed, separated by 1 to 10 cm-thick muddy beds (Figure 9, images 2, 3, and 4). The bottom of unit 2 is marked by a very distinct transition toward massive silty clay with sparse bioturbation, and a carbonate content >25% (Figure 6). In detail, this unit can be divided into

four coarsening-upward subunits, each displaying a coarsening upward pattern (Figure 11a).

[33] Seismic units U151 and U152 are characterized by a very poor faunal content. Rare worn fragments of bivalves are found together with partly reworked benthic foraminifera (mainly *Ammonia* sp. and *Elphidium* sp., Figure 10).

[34] 3. Surface D60 corresponds to 80 cm of very coarse-grained material, mainly composed of shell fragments (sedimentary unit 3). In detail, two coarse-grained intervals with an erosional base can be distinguished, separated by less than 10 cm of marine clay (Figure 11b). This interval is rich in molluscs but with low-diversity faunal assemblage dominated by *Abra* sp., *Corbula* sp., and *Turritella communis* (Figure 10).

[35] 4. U129 (sedimentary unit 4) is made of alternating beds of fine sand and bioturbated clay or silty clay, with rare laminations (Figure 7, section 47).

[36] 5. D55 is a 10 cm-thick with pebbles up to 2 cm in diameter.

[37] 6. U100 (sedimentary unit 5) displays highly bioturbated silty clay (Figure 9, image 6) and rare silt/fine sand beds (Figure 6 and Figure 7, section 61).

[38] 7. D50 is made of two coarse-grained intervals, about 50 cm-thick each, extremely rich in biogenic material (Figure 9, image 7), separated by a bioturbated fine-grained interval, with parallel laminations preserved in the sandy beds (sedimentary unit 6). Relatively high-diversity high-abundance molluscs assemblages are identified here (Figure 10) with species pertaining to bivalves (*Myrtea spinifera*, *Nucula* sp., *Nuculana commutate*), scaphopods (*Dentalium*), and the typical prodeltaic association *Turritella communis*-*Ditrupa arietina* (serpulids polychaetes).

[39] 8. U80 is a coarsening-upward sequence consisting (from top to bottom) in well-sorted fine to very fine sand (see grain size and gamma ray in Figure 6) with planar- and cross-bedding (sedimentary unit 7) passing to mud-sand alternations with intense bioturbation and occasional horizontal laminations (sedimentary unit 8; Figure 8, sections 88, 90, 91).

[40] 9. D45 is a 25 cm-thick interval of medium sand with abundant shell debris (sedimentary unit 9; Figure 9, section 9). Here, molluscs as *D. arietina* and *T. communis* are associated with the solitary

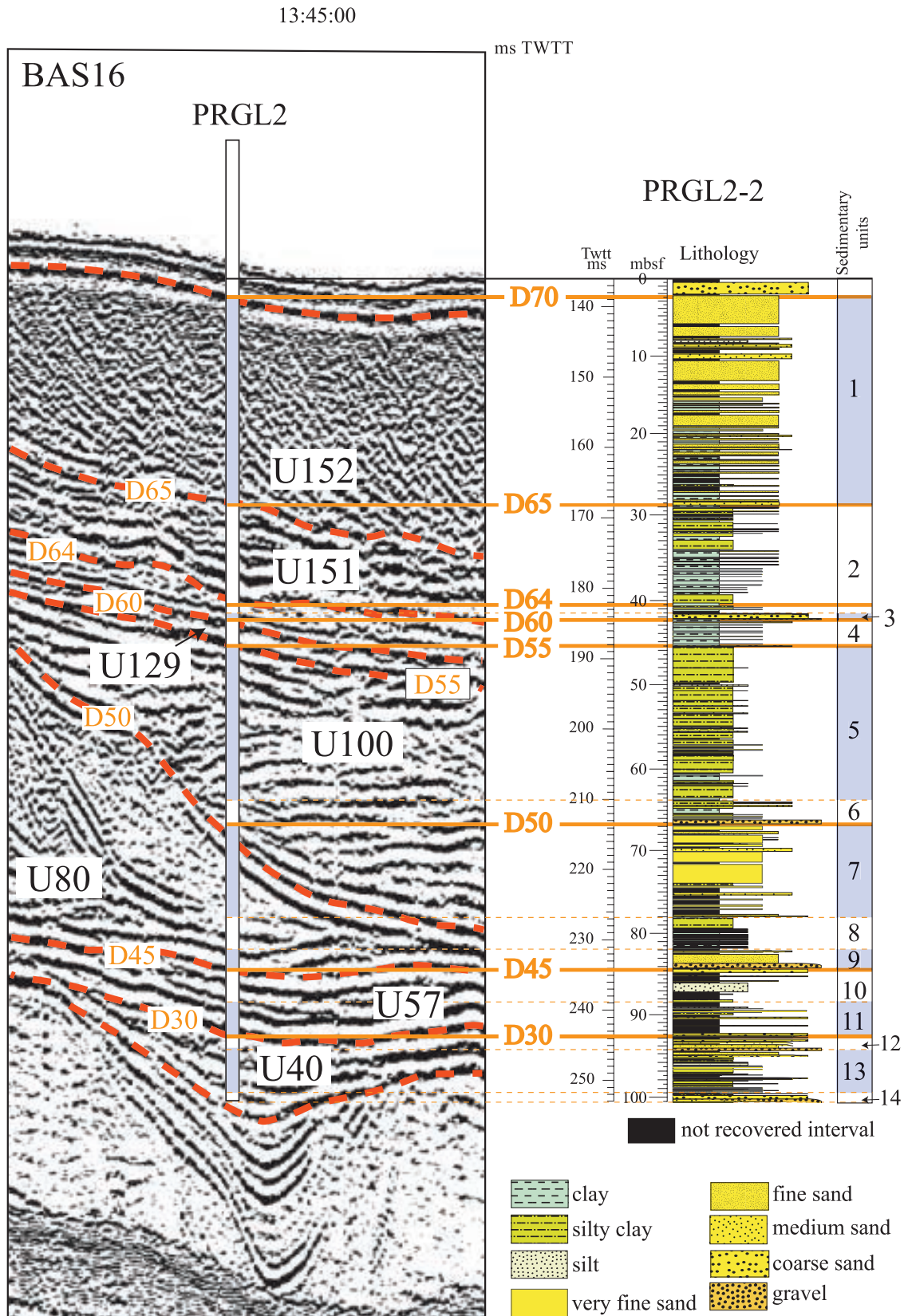


Figure 4. Correlation between seismic and lithological data after the conversion of mbsf depths into mstwtt on the basis of P wave velocities from MSCL. Sedimentary units 1–14 are detailed in Table S1 of the Auxiliary Material.

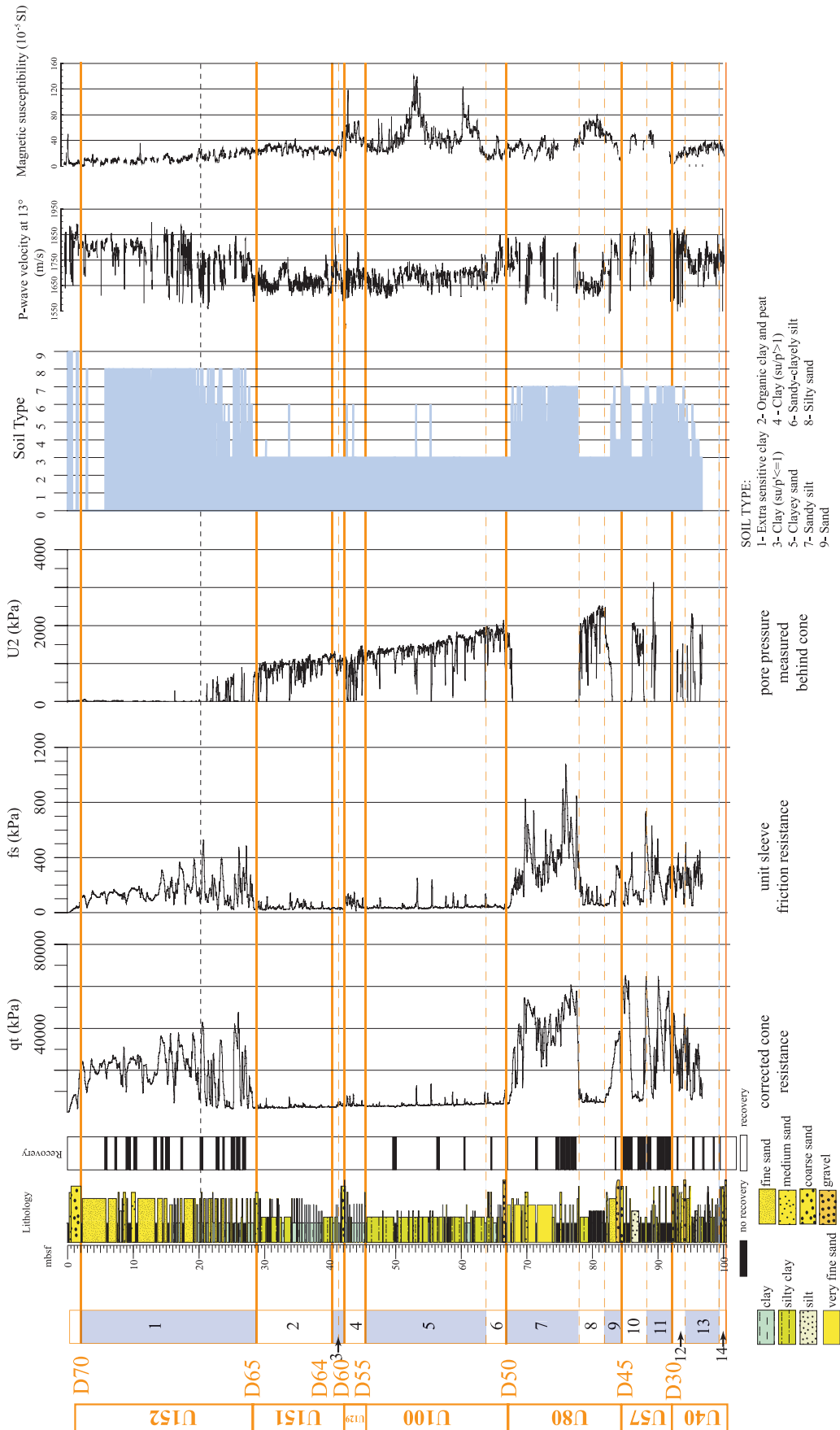


Figure 5

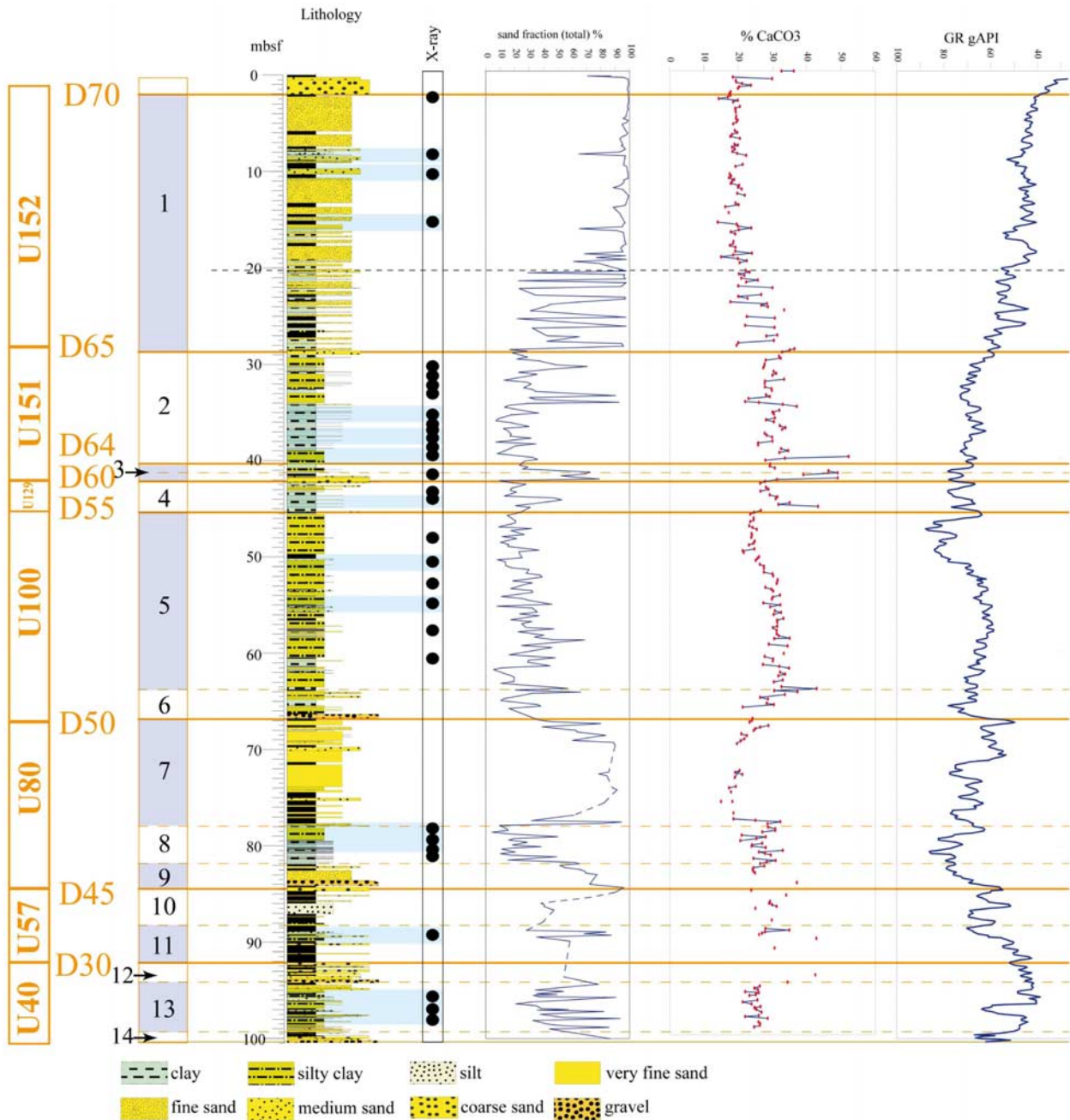


Figure 6. Total sand fraction, carbonate content, and natural gamma ray counts at PRGL2-2 and correlation with corresponding sedimentary units. Note that the grain size analysis only takes into account the <2 mm fraction; therefore gravel and shell beds are not shown in the vertical profile.

Figure 5. Geotechnical and physical properties measured at PRGL2-2 site. Lithological characteristics and soil types show an outstanding correspondence that can be used for lithological prediction of nonrecovered intervals. The main lithologies are estimated by the combination of resistance to cone penetration (qt) and friction resistance (fs) for sediments comprised between clay and medium sand. Thick coarse grained horizons are not evidenced by this methodology. Between 2 and 5.5 mbsf the lack of pore pressure measurements (due to the high permeability of sand) does not allow lithological properties to be established. In addition, slight discrepancies between lithological prediction and real lithology are observed (see transition between sedimentary units 1–2 and 6–7). In fact, the CPTU has been measured 3 m away from PRGL2-2 and lateral facies changes might be possible.

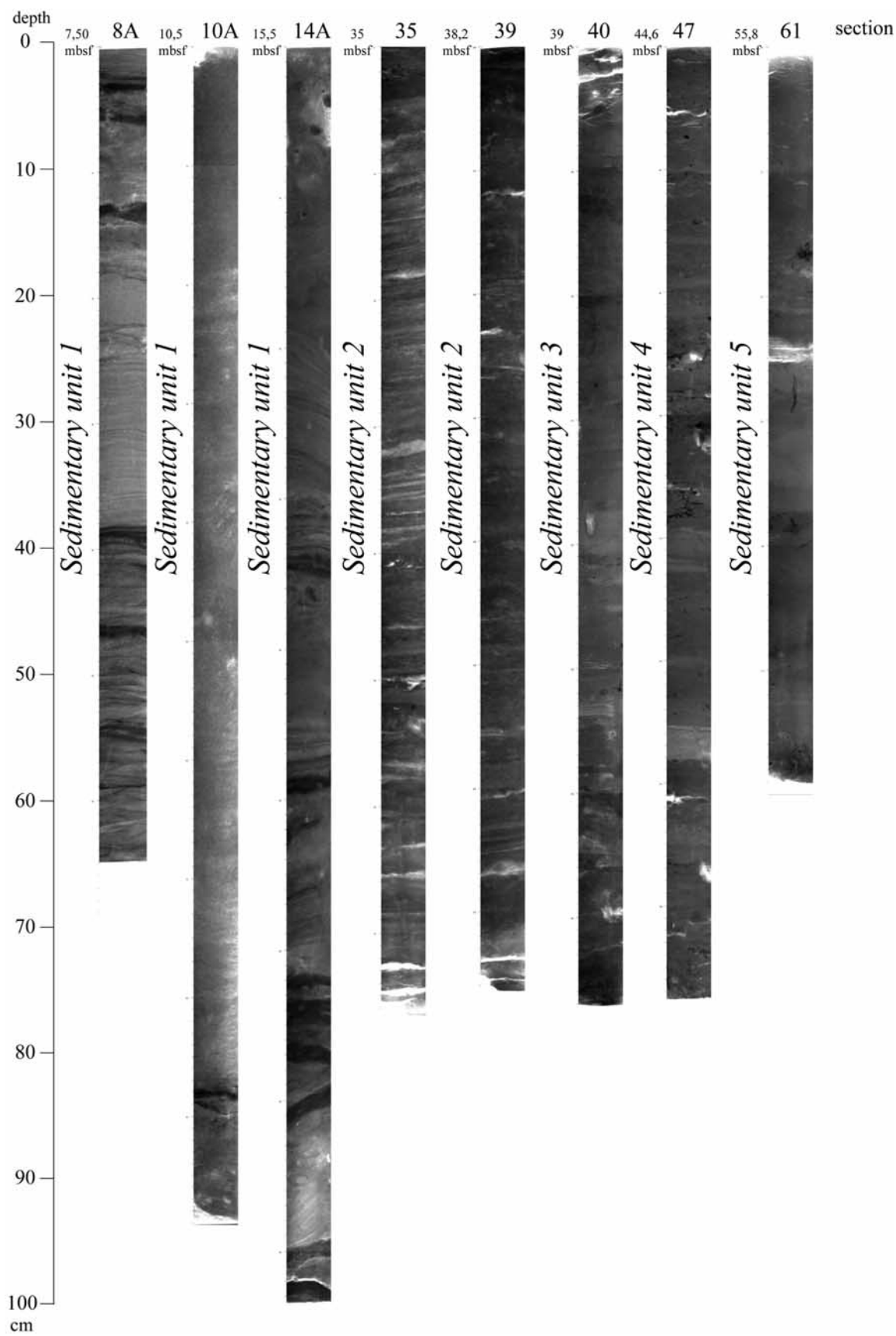


Figure 7

coral *Caryophyllia* and a number of bivalves e.g., Veneridae species, *Dosinia lupinus*, *Saccella commutata*, *Parvicardium* sp, *Mytilus* sp., etc.

[41] 10. U57 and U40 includes clayey silts (sedimentary units 10 and 13) and sandy/gravelly deposits (sedimentary units 11 and 12).

[42] 11. U40 consists of clayey silts with a very coarse interval (large rounded clasts and shell fragments) at the bottom of the borehole (sedimentary unit 14; Figure 11c, Figure 9, image 10) in a muddy sand matrix (Figure 8, section 114; Figure 9, image 10). Penetrometer cone resistance (*qt*, Figure 5) is widely used in this part of the borehole for lithological prediction because of poor recovery. It allowed us to distinguish slight lithological differences (medium to coarse sand).

[43] A high degree of reworking concerns the bioclasts (worn and chalky fragments), despite their abundance and diversity (Figure 10).

4.3. Chronostratigraphic and Biostratigraphic Constraints

4.3.1. ¹⁴C Dates

[44] Radiocarbon dating has been carried out for the first 42 m of the borehole that fall within the radiocarbon dating resolution (Table S2, Auxiliary Material).

[45] We obtained good results for the top of the borehole (U155) and for the fine-grained interval of seismic U151 (Figure 12), whereas significant age inversions affect the sandy interval of U152 (Figure 12). Within the ¹⁴C ages that are clearly distorted because of the occurrence of reworked material, it is worth noting that the measured ages show an overall trend from older (about 36 cal ka BP) to younger (26 cal ka BP) moving from the top to the bottom of the interval. Thus, rather than discarding them, we can use these data for discussing the nature of erosion during falling sea levels and eventually, the origin of sediments deposits during forced regression (see section 5).

4.3.2. Calcareous Nannoplankton

[46] Coccolithophore assemblages observed in the studied samples of PRGL2-2 are dominated by

Noelaerhabdaceae. Reworked nannofossils are a common feature of all studied samples and are even present in the samples that are almost barren of calcareous nannoplankton. The age of basal sediments remains undetermined because of poor preservation of nannoplankton in sedimentary units 7 to 14. However, significant events are identified in the upper layers that allow a correlation with the oxygen isotope stack of *Lisiecki and Raymo* [2005] (Figure 12).

[47] First occurrence of *Emiliania huxleyi* is identified at 60.56 mbsf. The age of this event was established by *Thierstein et al.* [1977] at 268 ka (top of MIS-8). It has to be taken into account that this first occurrence horizon (lower limit of the present-day Nannofossil Zone NN21 of *Martini* [1971]) could have been influenced by the low coccolithophore abundances in the samples.

[48] Another significant event is the age of the top of the hole. The coccolithophore assemblage compositions and the high abundances present in the uppermost interval indicate that this horizon is younger than the last glacial period (scarcity of *E. huxleyi* >4 μm).

[49] Finally, there are other events. Despite the low abundance of calcareous nannoplankton in most samples, the following horizons can be approximated (Figure 12):

[50] 1. Reversal in *Gephyrocapsa caribbeanica*/*Gephyrocapsa oceanica* - small *Gephyrocapsa*: *G. caribbeanica* and *G. oceanica* decrease their abundances and small *Gephyrocapsa* becomes the dominant group at about 62.93 mbsf. This event has been dated by *Villanueva et al.* [2002] and *Flores et al.* [2003] between 260 and 245 ka (top of MIS8).

[51] 2. Reversal in small *Gephyrocapsa*-*Gephyrocapsa muelleriae*: This last species increases in abundance around 43.73 mbsf. This probably approximates the event occurring during the middle of MIS6 (between 160 and 170 ka, as identified by *Villanueva et al.* [2002]).

[52] 3. Acme of *Emiliania huxleyi*/Reversal in *Gephyrocapsa muelleriae* - *Emiliania huxleyi*: The

Figure 7. X-ray images (see position in depth in Figures 4 and 6) evidencing sedimentary facies and structures: horizontal lamination and swaley cross-bedding (8A), bioturbated sand (10A), hummocks and associated parallel lamination (14A), bioturbated storms beds in mud (35, 39), bioturbated clays with rare laminated silty beds (40, 47 and 61).

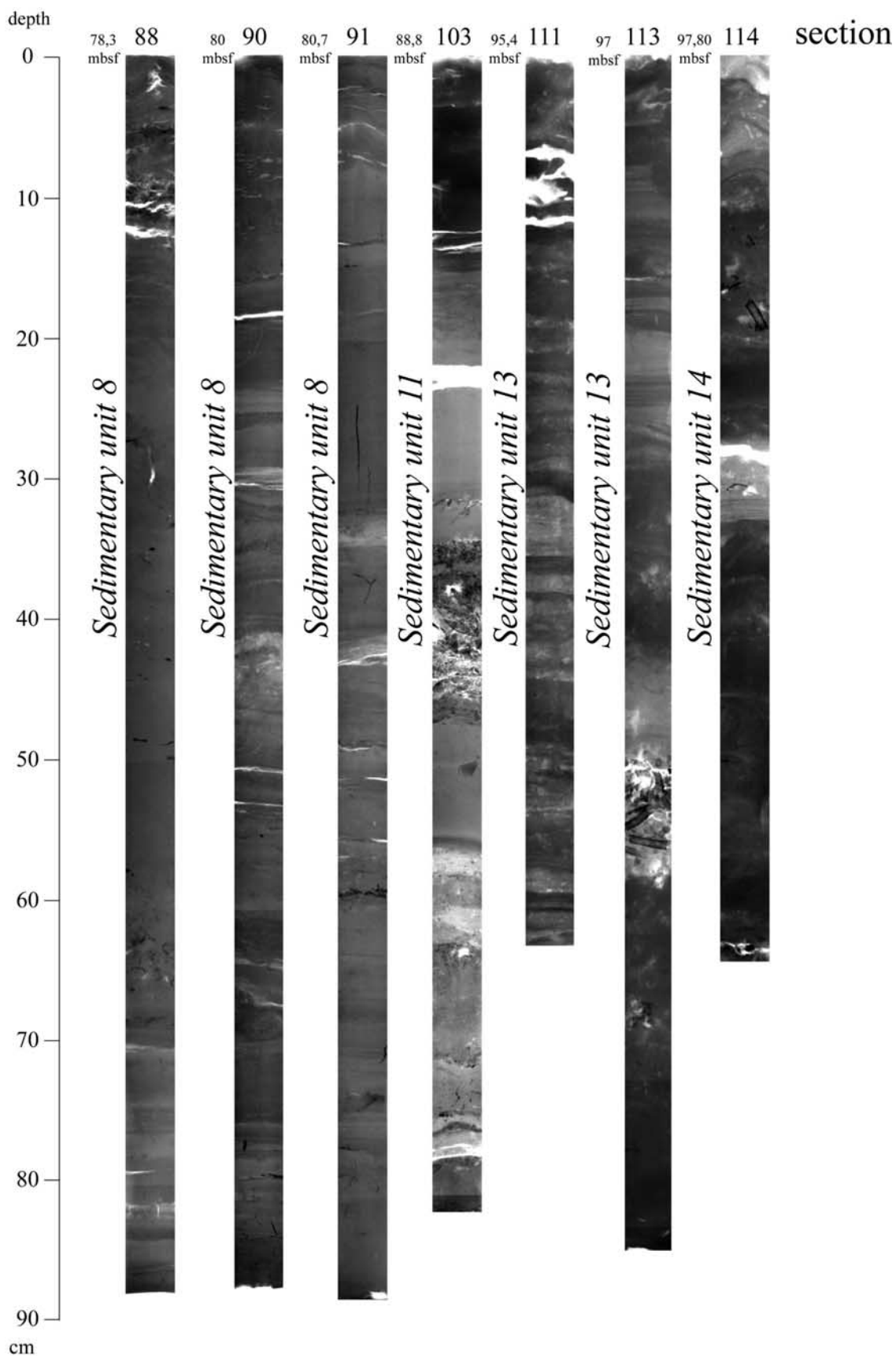


Figure 8

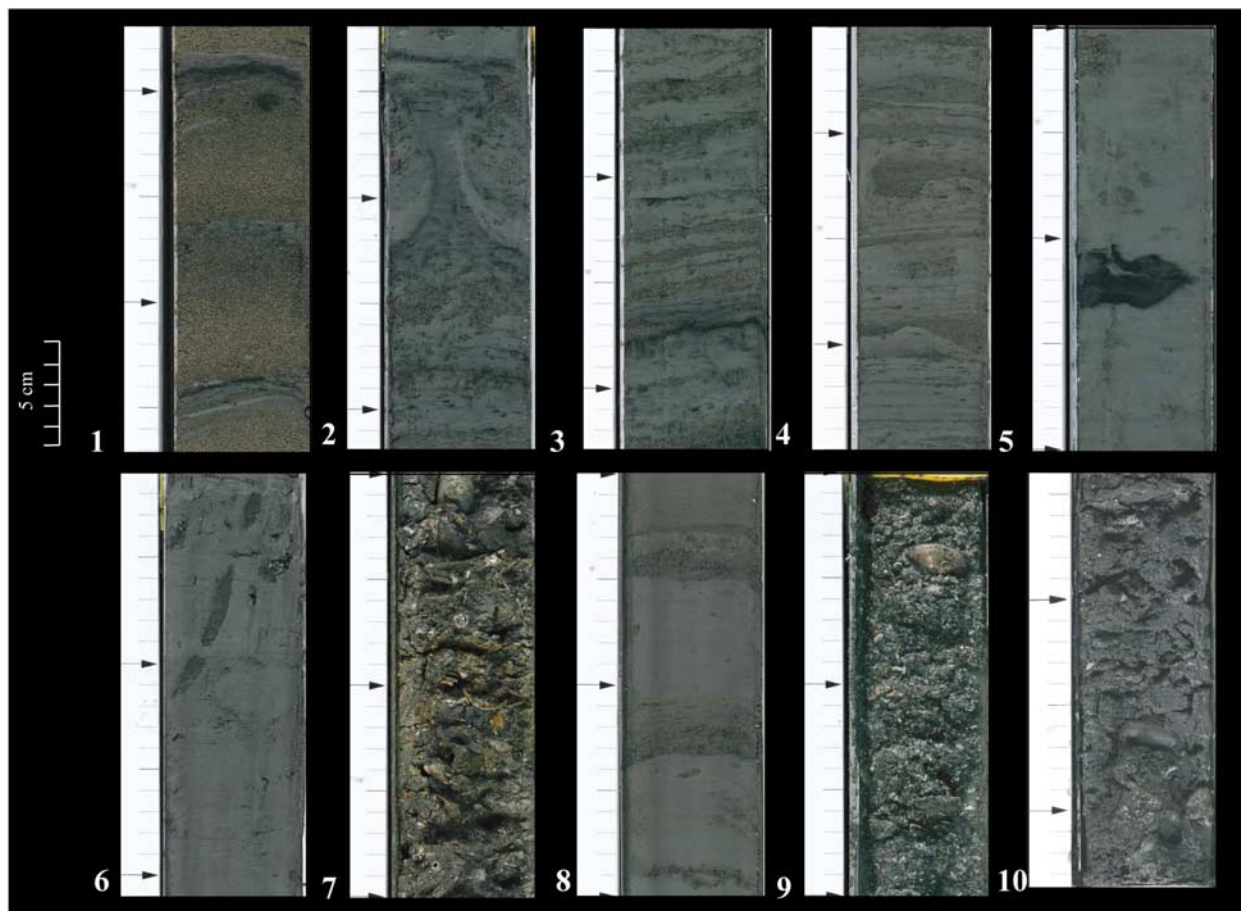


Figure 9. Photos from selected cores. Image 1 shows section 8B/37–57 cm (8.50–8.70 mbsf): mud intervals in massive sands; image 2 shows section 32/2–22 cm (32.61–32.80 mbsf): silty clay with fine sand beds, large burrow; image 3 shows section 34/23–43 cm (34.43–34.63 mbsf): Lenticular/wavy fine sand/silt beds and clay. Erosional basal contacts; image 4 shows section 36/25–45 cm (36.05–36.25 mbsf): lenticular (rippled?) fine sand beds and clay/silty clay. Some scours at the bottom of sand beds; image 5 shows section 40/30–50 cm (39.30–39.50 mbsf): Intensely bioturbated silty clay with organic matter spots; image 6 shows section 69/1–21 cm (62.21–62.40 mbsf): very bioturbated clay/silty clay; image 7 shows section 74/20–40 cm (66.40–66.60 mbsf): muddy bioclastic gravel; image 8 shows section 91/30–50 cm (80.94–81.10 mbsf): graded silty sand beds in silty clay; image 9 shows section 95/0–20 cm (83.60–83.80 mbsf): very coarse-coarse muddy sand with very abundant shells and shell fragments, including complete bivalves; image 10 shows section 116/64–84 cm (99.57–100.13 mbsf): Sandy gravel with large rounded clasts (up to 3 cm).

latter increases its abundance at about 41.34 mbsf, approximating the position of MIS4.

5. Discussion

[53] Integration of geophysical multiproxy borehole data allows us to propose a synthetic interpretation of Quaternary depositional units and

surfaces in the Gulf of Lions (Table S1, Auxiliary Material).

5.1. Nature and Origin of Major Erosion Surfaces

[54] A striking feature along PRGL2-2 is the perfect match between major seismic reflections (including the seafloor) and very coarse intervals

Figure 8. X-ray images (see position in depth in Figures 4 and 6) evidencing sedimentary facies and structures: intensively bioturbated clays with laminated sand beds (81), heterolithic facies (90 and 91 comparable to 35 and 39 in Figure 7), muddy shelly lag deposits with associated silty-sand bioturbated layers (103), alternating sand and mud couplets, slightly bioturbated (111), bioclastic material lag (worm tubes can be distinguished) with bioturbated clay passing upward to horizontally laminated silty clay (113), sand/clay alternations with sparse biogenic material (114).

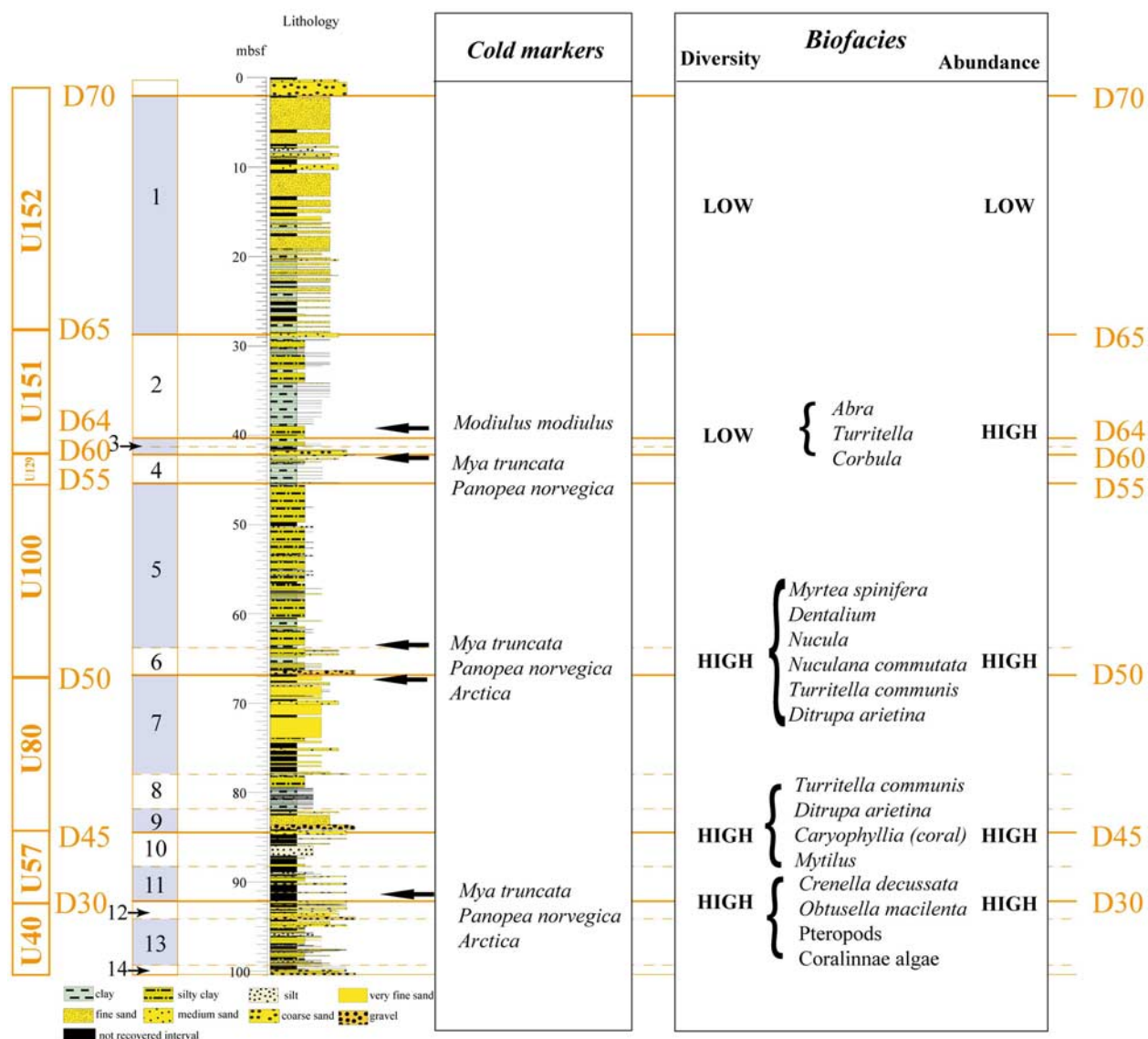


Figure 10. Synthetic scheme of mollusc assemblages examined in correspondence of erosion surfaces.

with shells and shell debris. The deposits with the richest mollusc content are associated with the major discontinuities. The mollusc assemblages are indicative of diverse environments, from open shelf to sublittoral, and are suggestive of an intense reworking. Cold-water Pleistocene species are found within D60, D50, D45, and D30 and described within D70 based on shallow cores [Bassetti et al., 2006].

[55] The boreoceltic guests have an important ecobiostratigraphic and climatic significance: *Modiolus modiolus*, *Arctica islandica*, cf. *Mya truncata*/*Panopea norvegica* known to proliferate in the Mediterranean only during glacial periods

[Malatesta and Zarlenga, 1986]. They occur consistently in association with major bounding surfaces. Interestingly, these cold-water species are in most cases mixed with temperate species. The borehole data confirm previous seismic and sequence stratigraphic interpretations that the major seismic discontinuities are polygenetic erosion surfaces formed as sequence boundaries at the top of prograding wedges, during sea level falls driven by 100 ka glacioeustatic cycles, and subsequently reworked by marine ravinement during sea level rises (see summaries in the work of Berné et al. [2004] and Rabineau et al. [2005]). The age of ~15 ka BP at the bottom of D70 found here (Figure 12) is consistent with ages

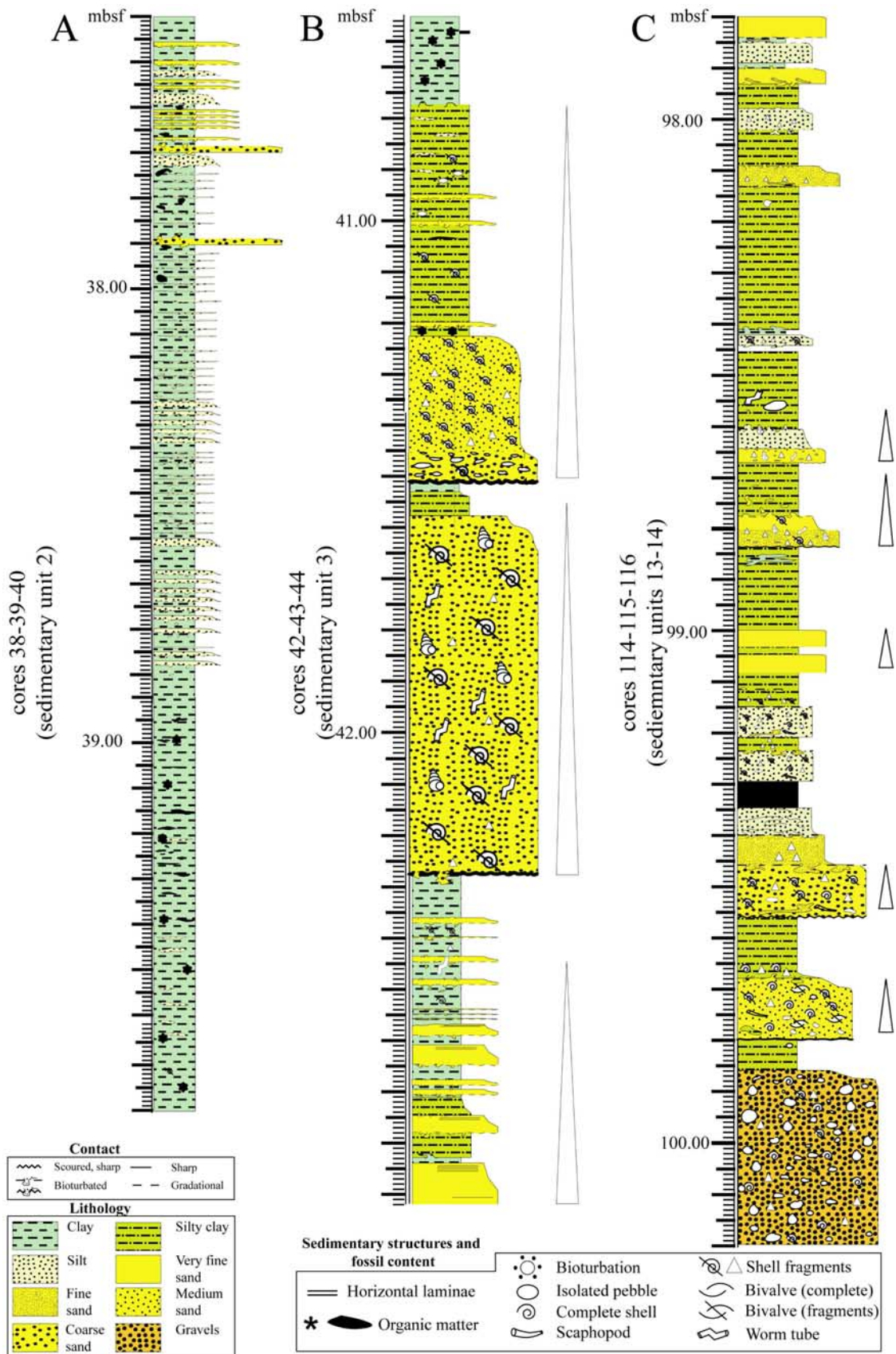


Figure 11

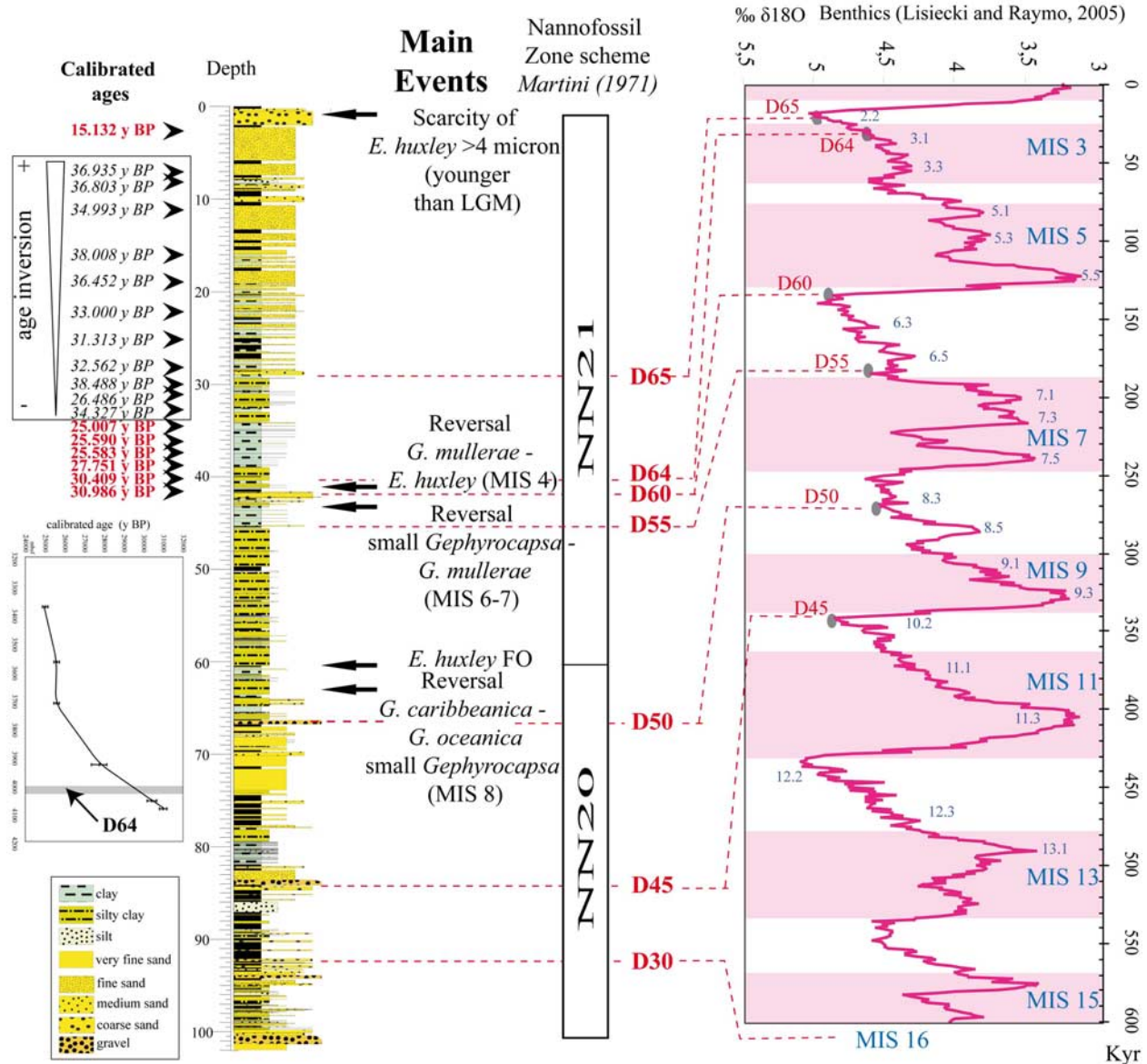


Figure 12. Chronostratigraphy of PRGL2-2 and correlation with the sea level curve [Lisiecki and Raymo, 2005]. ^{14}C dates provide an accurate chronology of the last sequence (U151–152). Deeper in the borehole, the detection of significant nannoplacton events are utilized down to MIS8. The bottom of the hole has been dated on the basis of seismic correlations with the PRGL1–4 borehole (see Figure 2).

given by Bassetti *et al.* [2006] and confirms that D70 was reworked by marine ravinement during the deglacial sea level rise.

[56] Transgressive deposits, which are very thin or absent on the outer shelf, except at the position of

sand ridges (U155 in Figure 3) are capped by condensed surfaces during highstands. This observation explains the significant mix of glacial and “warm” fauna living at different water depths. In details, sediments corresponding to seismic surfaces D60, D50, and D45 include in all cases two

Figure 11. Detailed logs of selected cores. (a) Part of a subunit of sedimentary unit 2 showing an overall coarsening upward pattern with storm-generated beds based by an interval of clay, intensively bioturbated and with an high content of organic matter; (b) Coarse grained interval of the sedimentary unit 3 (corresponding to seismic surface D60), consisting of two coarse-grained beds (with shells and heterogeneous biogenic material) separated by about 1 m of marine clays; (c) the fining upward basal coarse-grained interval (sedimentary unit 14) made of sand and gravel (channel infill deposits).



coarse-grained intervals, separated by 10 cm to 1 m of very fine sand or silty clay material. These fine-grained intervals might correspond to transgressive deposits separating a ravinement surface (at the base) and a condensed interval (maximum flooding surface, at the top), as described for D70 by *Bassetti et al.* [2006]. The reduced thickness (<1 m) of these transgressive deposits hampers their detection on seismic profiles.

[57] The lowermost bounding surface (D30) falls in a distinctive lithologic interval, with a coarse-grained basal unit (sedimentary unit 14) including material such as rounded pebbles implying the vicinity of a river. On seismic profiles, these deposits correspond to the infill of an axial incision within the Bourcart canyon. This supports the idea of a genetic link between axial incisions that downcut canyon heads and rivers during lowstands, as proposed by *Baztan et al.* [2005].

5.2. General Stratigraphic Organization

[58] Biostratigraphy allows us to propose a general chronostratigraphic and sequence stratigraphic interpretation of the study area. Major seismic units with steep clinoforms correspond to sandy shorefaces or delta fronts/prodeltas formed during major sea level falls and ensuing lowstands of each 100 ka glacial cycles. The age of seismic unit U100 (MIS6–7) is consistent with a MIS8 origin for seismic U80, immediately beneath. The perfect preservation of U80 (including preservation of the topsets of the clinoforms) can be explained by substantial accommodation space formed by erosion during the two previous low stands of the sea (MIS10 and MIS12), that were much more pronounced than MIS8. Within MIS6, three major subunits with thick (>20 m) and steep (>3°) clinoforms, labeled U95, U110, and U130, have been previously identified and mapped in three dimensions [*Rabineau et al.*, 2005, Figures 7 and 8]. Among these units, only U95 extends to the vicinity of the borehole (Figure 3), the others being situated in a more offshore and further east [*Rabineau et al.*, 2005]. In the absence of precise chronostratigraphic constraints, the origin of these multiple sand bodies within one single 100-ka falling stage systems tract could be attributed to purely autocyclic processes, such as switching of deltaic lobes in a supply dominated environment, with stable sea level being. However, considering that there is at least a difference of 30 m in the depths of the topsets of clinoforms of units U95 and U130 [*Rabineau et al.*, 2005], it is more reasonable to invoke an allocyclic

(sea level fall) origin. In this view, the lowstands corresponding to MIS6.6, MIS6.4, and MIS6.2 could be good candidates for the formation of U95, U110, and U130, respectively.

5.3. Nature and Significance of Large Clinoforms of U151/U152

[59] The full recovery of sediments from seismic unit U151/U152, as well as the availability of precise time constraints (from absolute ¹⁴C dates) for this interval allows discussion of the origin of large-scale clinoforms. These features have been often described from seismic data on many continental shelves but rarely sampled. Comparison with similar features from ancient stratigraphic record adds another interest to our results.

5.3.1. Synthesis of Sedimentological and Biostratigraphic Information on U151/U152

[60] The sedimentary facies association within U151/U152 represents a typical coarsening upward trend commonly described on wave-dominated shelves [*Walker and Plint*, 1992], with the vertical superposition of three main facies (from top to bottom):

[61] 1. The first is planar to very low-angle stratified sand and possibly swaley cross-stratification (Figure 7, sedimentary unit 1, section 8A), indicative of efficient wave reworking. This deposit lies above an intensely bioturbated unit (Figure 7, sedimentary unit 1, section 10A).

[62] 2. The second is cross-stratified, well-sorted fine sands with parallel to low-angle converging laminations suggesting a possible hummocky cross-stratification (Figure 7, sedimentary unit 1, section 14A). The HCS unit represents deposition above storm but probably not far from wave base [*Dumas and Arnott*, 2006].

[63] 3. The third is bioturbated mud with interbedded thin sand beds (Figure 7, sedimentary unit 2, sections 35 and 39). Storm-generated event beds, intensively bioturbated with sharp erosional base, corresponding to moderate-energy storm-dominated shelf zone with fair weather mud drapes [*Aigner and Reineck*, 1982].

[64] The mutual stratigraphic position of these facies strongly supports the interpretation of U151/U152 as a regressive complex including foreshore and shoreface (and/or delta front/prodelta) domains. Sedimentary unit 1 is characterized by a high-energy (coastal) setting marked essentially by (1) massive,



well-sorted fine to medium sand with low carbonate content; (2) horizontal lamination and possible swaley cross-stratification, indicative of winnowing by wave action; (3) possible hummocky cross-stratification indicative of a storm-dominated lower shoreface environment.

[65] Storm beds are preferably recorded in the “offshore” facies (bottomsets, sedimentary unit 2) as testified by highly heterolithic deposits, mainly consisting of fine-grained beds alternating with repeated, distally deposited, storm beds. Bioturbation of the finer section (silty clay) indicates prolonged intervals of calm conditions between the deposition of tempestites. It has been argued that the so-called “offshore muds” do not really exist and are in fact part of the lower shoreface domain because mud is trapped along shore by shelf circulation [Dalrymple and Cummings, 2005]. This is exactly what is observed in the Gulf of Lions, where mud is confined on the inner shelf [Berne et al., 2007]. We therefore consider sedimentary unit 2 as part of the lower shoreface/prodelta domains.

5.3.2. Integration of Sedimentological and Seismic Data

[66] The upper 20 m massive sands of sedimentary unit 1 correspond to the steep (up to 5°) foresets of seismic unit U152. They pass progressively to sands with thin muddy interbeds between 20 and 30 mbsf where clinoforms are dipping more gently. The abrupt deepening of sedimentary facies below 30 mbsf corresponds to seismic surface D65. The alternating bioturbated sands and muds observed below this surface (sedimentary unit 2) correspond to the bottomsets of clinoforms of unit U151. Despite the dominant sandy lithology of clinoforms, the impedance contrast that is at the origin of reflectors on seismic profiles (foresets of U152) is likely due to the presence of centimeter-thick clayey layers or packets of such layers.

[67] Sedimentary structures and paleoenvironmental indications given by fauna and microfauna confirm earlier interpretations, based on seismic stratal architectures (Aloisi [1986] and subsequent workers): U151 and U152 represent wave-dominated shorefaces deposited during an overall sea level fall at the end of the last glacial cycle.

[68] The shoreface deposits observed here differ from typical shoreface modern deposits (highstand), which commonly show much gentler angle of clinoforms (0.3° on average [Walker and Flint,

1992], about 0.5° on the modern Sète shoreface [Barousseau et al., 1994]). On the other hand, examples of clinoforms with steep dip angles are reported in the stratigraphic record in forced regressive shelf margins [Hanken et al., 1996; Hart and Long, 1996; Massari et al., 1999; Surlyk and Noe-Nygaard, 2005]. Quaternary margins worldwide also document examples of sandy (or supposedly sandy) shelf or shelf-edge shoreface or deltaic clinoforms with angles of dip similar to that of the Gulf of Lions' shorefaces [Anderson et al., 2004; Chiocci and Orlando, 1996; Hernandez-Molina et al., 1994; Hiscott, 2001; Suter and Berryhill, 1985; Sydow et al., 1992; Trincardi and Field, 1991; Trincardi and Correggiari, 2000; Winn et al., 1998]. Possibly, the difference in slope angles between present-day shorefaces and Pleistocene/Ancient indicates that the latest record progradation with more abundant sand supply, whereas modern examples correspond to equilibrium profiles of sand-starved shorelines-shelf system. An alternative (or additional) explanation is that these shorefaces could in fact correspond to the “asymmetric wave-dominated deltas” that form updrift of deltaic systems subject to longshore drift [Bhattacharya and Giosan, 2003]. Such an asymmetry has been described on the modern Po delta [Correggiari et al., 2005]. The steep dip angle of the clinoforms measured on seismic profiles is consistent with slope measured on the modern delta front of the active Roustan distributary channel of the Rhone, i.e., about 4° [Maillet et al., 2006]. Another alternative explanation has been proposed by F. Trincardi (personal communication, 2006), these sand bodies being interpreted as the product of along-shore sediment advection to deeper areas of increased accommodation, as documented for the muddy regressive deposits on the Adriatic [Cattaneo et al., 2007].

[69] The thickness of the Gulf of Lions' shoreface deposits is also quite different from values reported from modern examples. It reaches up to 30 m for U152 (including 20 m of massive sands), and even 40 m for U80 (where sand thickness is estimated to be more than 30 m). These values have to be compared to the thickness of Holocene shorefaces, which are in the range of 10–20 m [Hampson and Storms, 2003]. On the other hand, they are comparable to the thickness of some ancient shoreface deposits such as the Kenilworth Member of the Book Cliffs [Pattison and Walker, 1995]. An explanation for this difference is that modern shorefaces prograde over inner shelves where accommodation is limited because of the low gradi-



ent, whereas the shorefaces studied here developed at the shelf edge. In addition, the steep clinoforms of U151/152 and U80 developed immediately seaward of a step in the underlying surface (Figure 2). Probably this step provided additional accommodation for shoreface deposition, as proposed by *Trincardi and Field* [1991] for Tyrrhenian Sea shorefaces, or as observed at the outcrop scale by *Massari et al.* [1999].

[70] In addition to this morphological control, *Hampson and Storms* [2003] proposed that the main processes (or recurrence of processes) controlling the architecture of modern and ancient shorefaces are substantially different: modern shorefaces represent a much shorter time span and therefore are mainly controlled by wave climate and/or sediment supply; in contrast, shorefaces from the geological record a shoreline trajectory [*Helland-Hansen and Martinsen*, 1996] during changing rate of relative sea level rise. This could account both for the greater thickness of ancient shorefaces and for differences in clinoform dip angles. The available chronostratigraphic framework allows us to sustain this hypothesis.

5.4. Regressive Downward Stepping Parasequences Linked to Pulsed Sea Level Falls

[71] U151 and U152 were deposited during the overall sea level fall that took place between the highest sea level of Marine Isotope Stage (MIS) 3 (around 50 ka BP) and the lowest sea level of MIS2 (Last Glacial Maximum), around 22 cal ka BP. Even if the position of global sea level during MIS3 is still debated (ranging from -35 m to -95 m, see compilation of sea level curves in the work of *Jouet et al.* [2006], the MIS3-MIS2 interval record a period of overall cooling trend accompanied by lowering of sea level, punctuated by rapid climate changes generally referred to as Dansgaard Oeschger (D/O) cycles [*Bond et al.*, 1993; *Dansgaard et al.*, 1993], with Heinrich Events (HE) [*Heinrich*, 1988] occurring at the end of some of the coldest stadials.

[72] In the lithological succession within U152/U151, we observed coarsening upward units indicative of a general regressive pattern that appear separated by flooding surfaces mantled by fine-grained sediment. In particular, such flooding surfaces are observed at about 29 and 40 mbsf which correspond to seismic reflections D64 and D65 and are indicated by sedimentary facies suggesting a relatively abrupt deepening as marked in Figure 13.

[73] The chronostratigraphic constraints obtained from shallow cores (~ 20 m long) retrieved landward and seaward of PRGL2-2 [*Jouet et al.*, 2006], as well as the ^{14}C dates obtained within U151/152 at PRGL2-2 imply that (1) D65 formed between 24.13 and 22.7 cal ka BP (from *Jouet et al.* [2006]) a time frame consistent with an age < 25 cal ka BP found at 33.75 mbsf on PRGL2-2, about 4 m below the position of D65 (considering an average sedimentation rate of 1 m/ka); and (2) D64 formed between 30.4 and 27.75 cal ka BP (if we assign a depth of about 40 mbsf for D64 at the position of this borehole).

[74] Finally, the ages of both surfaces fall within the time intervals assigned to HE 2 and HE 3 (~ 24 and 30 ka cal BP, respectively [*Hemming*, 2004]). They also correspond to the end of marked periods of sea level falls (in the order of 10 m) observed in the Red Sea [*Arz et al.*, 2007; *Siddall et al.*, 2003].

[75] On seismic profiles, a very pronounced downward shift surface corresponds to seismic surface D63, that marks a very distinct erosional boundary between bottomsets of U147 and steep (probably sandy) clinoforms of U151 (Figure 13). At the resolution of seismic data, this surface is merged with the main sequence boundary (D60); however, we notice a distinctive fine-grained interval separating two very coarse intervals interpreted as ravinement surfaces. This interval has not been dated on PRGL2-2. However, it was dated previously in a piston core at ~ 41 cal ka BP [*Jouet et al.*, 2006], whereas an age of ~ 38 cal ka BP is found at the deep borehole PRGL1-4. The relevance of the erosion linked to D63, as it is seen on seismic profiles, can be explained by a much higher magnitude of sea level drop between 43 and 40 ka cal BP (about 30 m according to *Arz et al.* [2007]). According to these authors, the magnitude of the ensuing sea level rise was in the same order (Figure 13), within only ~ 2 ka (about 1.5 cm/a), i.e., a rate in the same range as that of meltwater pulses during the last deglacial. The stratigraphic expression of this rapid transgressive interval could be the thin silt and clay layer situated at 41.51–41.56 mbsf between two coarse-grained intervals (Figure 11b), immediately above D60.

[76] Finally, within the prograding shoreface deposits recording the overall sea level fall between MIS3 and MIS2 display a sedimentary motif linked to higher-order incremental sea level falls and subsequent rises (Figure 13) that erode the

upper and seaward terminations of previous deposits and initiate a new phase of forced regression. These minor bounding surfaces, created by these pulsations are genetically similar to the major bounding surfaces, in the sense that they represent surfaces linked both to a fall and rise of sea level, but their lithologic expression is different from that of major bounding surfaces (D60, D50, D45, D30) because the magnitude of sea level changes and duration of processes at their origin are shorter. This scenario also allows the explanation of the age inversion observed within the ^{14}C data from U152. In the context of general sea level fall, the uppermost clinoform samples are sourced from deposits reworked from the entire emerged shelf (and therefore older on average). On the other hand, the deepest clinoforms correspond to a period of higher sea level and include less reworked material.

[77] Our scenario of shoreface preservation in response to pulsed sea level falls is quite similar to that proposed from the interpretation of ancient shoreface deposits. The concept was initially proposed by *Plint* [1988] and subsequently developed and applied to several ancient examples [*Hunt and Tucker*, 1992; *Mellere and Steel*, 2000; *Posamentier and Allen*, 1993; *Walker and Plint*, 1992]. A synthesis of the stratigraphic expression of such “falling stage systems tracts” is given by *Plint and Nummedal* [2000]. In the rock record, good examples of downstepping clinoform units separated by ravinement surfaces, very similar to our Gulf of Lions shoreface deposits, are given for instance by *Surlyk and Noe-Nygaard* [2005] from the lowermost Cretaceous of East Greenland. In modern (late Holocene) shoreface deposits, the effect of rapid, even if limited, sea level falls (<1 m, in this case in relation with tectonic uplift) is well documented by *Tamura et al.* [2007] who show intrashoreface erosion following tectonically induced sea level falls. Such surfaces are also reproduced by numerical experiments through sea level fall and/or increase of the wave height [*Storms and Hampson*, 2005]. The thickness of our shelf-edge shorefaces (compared to most of modern examples) could be ascribed to increased space available at the shelf edge, simply for geomorpho-

logic reasons, or to intense erosion during part of MIS3.

6. Summary and Conclusions

[78] 1. The prograding bodies in the Gulf of Lions are formed by massive sand with clinoforms dipping at 5° maximum and showing a progressive transition to silt to silty clay deposits basinward that form coarsening-upward sedimentary sequences. The sedimentological motif of these deposits is summarized in Figure 13.

[79] 2. These sand bodies formed during the overall sea level falls of the 100-ka glacial-interglacial cycles.

[80] 3. They are bounded by easily recognizable erosional surfaces that display a common sedimentological expression (coarse grained material, shell, and shell hash with species indicative of a variety of marine environments). Macrofauna (molluscs, corals) together with the lithological characteristics prove that these surfaces have a polygenetic origin (marine regressive erosion, subaerial erosion, marine transgressive ravinement and possible condensation during highstands). These surfaces form the major bounding surfaces recording 100-ka glacial-interglacial cycles. In several cases, mud deposits, 0.1 to 1 m thick are intercalated in these coarse beds and might represent transgressive deposits, not detected on seismic profiles.

[81] 4. Owing to the composite shape of the sea level curve, higher-frequency climatic cycles (20 and 40 ka) are also preserved in the form of prograding shoreface wedges. This is probably the case for MIS6.2, 6.4, and 6.6.

[82] 5. Our results differ from those of the Adriatic sites of PROMESS [*Ridente et al.*, 2008] where shelf deposits are mainly composed of prograding interglacial fine-grained deposits, due to increased southward advection of sediments from the Po during highstands of sea level.

[83] 6. Within the last glacial/interglacial sequence, cyclic changes of sedimentary environments show that the clinostratified bodies are composed of

Figure 13. Synthetic interpretation of the last forced-regressed unit (last 100 ka glacial-interglacial cycle between D60 and the seafloor) showing the stratigraphic signature of higher-order, stepped sea level falls creating second-order bounding surfaces (D63, D64, D65). Note the good match between the ages of these surfaces and the Heinrich events 4, 3, 2, respectively. D63, in particular, shows a drastic shallowing of sedimentary facies that could be explained by the 30 m sea level fall measure by *Arz et al.* [2007] in Red Sea. For clarity, post LGM deposits (U155) have not been represented.



several higher-order (para)sequences, bounded by flooding surfaces. Radiocarbon dates indicates that these minor bounding surfaces record rapid sea level changes during the overall MIS3-MIS2 sea level fall, in phase with the high-resolution isotopic records of the Red Sea [Arz *et al.*, 2007; Siddall *et al.*, 2003].

[84] 7. Each parasequence (about 40 m thick, including about 20 m of massive sand) formed within about 5–10 ka, and progradation during this interval was in the range of 1–2 km. The sea level drops that triggered progradation were of the order of 10–30 m.

[85] 8. The detection of river-derived material at the bottom of the borehole (unit 14), testifies the direct influence of fluvial discharge events at the shelf edge. This is the first evidence in this area of a connection between a lowstand river drainage and a canyon.

Acknowledgments

[86] The drilling operation was conducted within the European project PROMESS 1 (contract EVR1-CT-2002-40024). Data were processed and interpreted with the support of the French Agence Nationale de la Recherche (ANR, contract NT05-3-42040). Initial support for seismic data acquisition was provided by Ifremer, the French “Margins” program, and the EC-funded Eurostrataform project (contract EVK3-2001-00200). Engineers of FUGRO-BV and the captain and crew of the Amige drilling vessel *Bavenit* are warmly thanked for their dedication during the cruise. The European Promess shipboard party (<http://www.pangaea.de/Projects/PROMESS1>) and colleagues at Ifremer (A.S. Alix, F. Duval, G. P. Fernagu, G. Floch, N. Frumholtz, B. Marsset, L. Morvan, D. Pierre, M. Rovere, E. Thereau, Y. Thomas) are also thanked for various contributions during all phases of data acquisition and processing. A. Ceregato (University of Bologna) is thanked for revising the mollusc taxonomy. The authors of this paper are indebted to G-cubed Editors L.D. Labeyrie and V. Salters, Associate Editor F. Trincardi, as well as to G. Plint and an anonymous reviewer, for their thorough review of the manuscript. This is IGM contribution 1596. The first author benefited from fellowships from Eurostrataform and ANR at IFREMER (Centre de Brest).

References

Aigner, T., and H.-E. Reineck (1982), Proximity trends in modern storm sands from the Helgoland Bight (North Sea) and their implication for basin analysis, *Senckenb. Marit.*, *14*, 183–215.

Aloisi, J. C. (1986), Sur un modèle de sédimentation deltaïque: Contribution à la connaissance des marges passives, doctoral thesis, 162 pp., Univ. of Perpignan, Perpignan, France.

Anderson, J. B., A. Rodriguez, K. C. Abdulah, R. H. Fillon, L. A. Banfield, H. A. McKeown, and J. S. Wellner (2004), Late Quaternary Stratigraphic evolution of the northern Gulf

of Mexico margin: A synthesis, in *Late Quaternary Stratigraphic Evolution of the Northern Gulf of Mexico Margin*, edited by J. B. Anderson and R. H. Fillon, pp. 1–23, Soc. for Sediment. Geol., Tulsa, Okla.

Arz, H. W., F. Lamy, A. Ganopolski, N. Nowaczyk, and J. Patzold (2007), Dominant Northern Hemisphere climate control over millennial-scale glacial sea-level variability, *Quat. Sci. Rev.*, *26*(3–4), 312–321, doi:10.1016/j.quascirev.2006.07.016.

Austin, J. A., et al. (1998), *Proceedings of the Ocean Drilling Program, Initial Report 174A*, Ocean Drill. Program, College Station, Tex.

Bard, E., M. Arnold, B. Hamelin, N. Tisnerat-Laborde, and G. Cabioch (1998), Radiocarbon calibration by means of mass spectrometric ²³⁰Th/²³⁴U and ¹⁴C ages of corals. An updated data base including samples from Barbados, Mururoa and Tahiti, *Radiocarbon*, *40*(3), 1085–1092.

Barusseau, J. P., M. Radulescu, C. Descamps, C. Akouango, and A. Gerbe (1994), Morphosedimentary multiyear changes on a barred coast (Gulf of Lions, Mediterranean Sea, France), *Mar. Geol.*, *122*, 47–62, doi:10.1016/0025-3227(94)90204-6.

Bassetti, M. A., G. Jouet, F. Dufois, S. Berne, M. Rabineau, and M. Taviani (2006), Sand bodies at the shelf edge in the Gulf of Lions (western Mediterranean): Deglacial history and modern processes, *Mar. Geol.*, *234*, 93–109, doi:10.1016/j.margeo.2006.09.010.

Baztan, J., S. Berne, J. L. Olivet, M. Rabineau, D. Aslanian, M. Gaudin, J. P. Rehault, and M. Canals (2005), Axial incision: The key to understand submarine canyon evolution (in the western Gulf of Lion), *Mar. Pet. Geol.*, *22*(6–7), 805–826, doi:10.1016/j.marpetgeo.2005.03.011.

Berné, S., and C. Gorini (2005), The Gulf of Lions: An overview of recent studies within the French ‘Margins’ programme, *Mar. Pet. Geol.*, *22*(6–7), 691–693, doi:10.1016/j.marpetgeo.2005.04.004.

Berné, S., G. Lericolais, T. Marsset, J. F. Bourillet, and M. de Batist (1998), Erosional shelf sand ridges and lowstand shorefaces: Examples from tide and wave dominated environments of France, *J. Sediment. Res.*, *68*(4), 540–555.

Berné, S., M. Rabineau, J. A. Flores, and F. J. Sierro (2004), The impact of Quaternary global changes on strata formation. Exploration of the shelf edge in the northwest Mediterranean Sea, *Oceanography*, *17*(4), 92–103.

Berne, S., G. Jouet, M. A. Bassetti, B. Dennielou, and M. Taviani (2007), Late Glacial to Preboreal sea-level rise recorded by the Rhone deltaic system (NW Mediterranean), *Mar. Geol.*, *245*(1–4), 65–88, doi:10.1016/j.margeo.2007.07.006.

Bhattacharya, J. P., and L. Giosan (2003), Wave-influenced deltas: Geomorphological implications for facies reconstruction, *Sedimentology*, *50*(1), 187–210, doi:10.1046/j.1365-3091.2003.00545.x.

Bond, G. C., W. Broecker, S. Johnsen, J. McManus, L. Labeyrie, J. Jouzel, and G. Bonani (1993), Correlations between climate records from North Atlantic sediments and Greenland ice, *Nature*, *365*(6442), 143–147, doi:10.1038/365143a0.

Brookfield, M. E. (1977), The origin of bounding surfaces in ancient eolian sandstones, *Sedimentology*, *24*, 303–332, doi:10.1111/j.1365-3091.1977.tb00126.x.

Cattaneo, A., F. Trincardi, A. Asioli, and A. Correggiari (2007), The Western Adriatic shelf clinoform: Energy-limited bottomset, *Cont. Shelf Res.*, *27*(3–4), 506–525, doi:10.1016/j.csr.2006.11.013.



- Chiocci, F. L., and L. Orlando (1996), Lowstand terraces on Tyrrhenian Sea steep continental slopes, *Mar. Geol.*, *134*, 127–143, doi:10.1016/0025-3227(96)00023-0.
- Correggiari, A., A. Cattaneo, and F. Trincardi (2005), The modern Po Delta system: Lobe switching and asymmetric prodelta growth, *Mar. Geol.*, *222–223*, 49–74, doi:10.1016/j.margeo.2005.06.039.
- Dalrymple, R. W., and D. I. Cummings (2005), The offshore transport of mud: Why it doesn't happen and the stratigraphic implications, paper presented at Annual Meeting, Geol. Soc. of Am., Boulder, Colo.
- Dansgaard, W., S. J. Johnsen, H. B. Clausen, N. S. Dahl-Jensen, C. U. Hammer, C. S. Hvidberg, J. P. Steffensen, A. E. Sveinbjörnsdóttir, J. Jouzel, and G. C. Bond (1993), Evidence for general instability of past climate from a 250-kyr ice-core record, *Nature*, *364*, 218–220, doi:10.1038/364218a0.
- Davis, R. A., and P. B. Balson (1992), Stratigraphy of a North Sea tidal sand ridge, *J. Sediment. Petrol.*, *62*(1), 116–121.
- Dumas, S., and R. W. C. Arnott (2006), Origin of hummocky and swaley cross-stratification. The controlling influence of unidirectional current strength and aggradation rate, *Geology*, *34*(12), 1073–1076, doi:10.1130/G22930A.1.
- Flores, J.-A., M. Marino, F. J. Sierro, D. A. Hodell, and C. D. Charles (2003), Calcareous plankton dissolution pattern and coccolithophore assemblages during the last 600 kyr at ODP Site 1089 (Cape Basin, South Atlantic): Paleocceanographic implications, *Palaeogeogr. Palaeoclimatol. Palaeoecol.*, *196*(3–4), 409–426, doi:10.1016/S0031-0182(03)00467-X.
- Hampson, G. J., and J. E. A. Storms (2003), Geomorphological and sequence stratigraphic variability in wave-dominated, shoreface-shelf parasequences, *Sedimentology*, *50*, 667–701, doi:10.1046/j.1365-3091.2003.00570.x.
- Hanken, N.-M., R. G. Bromley, and J. Miller (1996), Plio-Pleistocene sedimentation in coastal grabens, north-east Rhodes, Greece, *Geol. J.*, *31*(4), 393–418, doi:10.1002/(SICI)1099-1034(199612)31:4<393::AID-GJ712>3.0.CO;2-H.
- Harms, J. C., J. B. Southard, D. R. Spearing, and R. G. Walker (1975), *Depositional Environments as Interpreted From Primary Sedimentary Structures and Stratification Sequences*, 161 pp., Soc. of Econ. Paleontol. and Mineral., Dallas, Tex.
- Hart, B. S., and B. F. Long (1996), Forced regressions and lowstand deltas: Holocene Canadian examples, *J. Sediment. Res.*, *66*(4), 820–829.
- Heinrich, H. (1988), Origin and consequences of cyclic ice rafting in the northeast Atlantic Ocean during the past 130,000 years, *Quat. Res.*, *29*(2), 142–152.
- Helland-Hansen, W., and O. J. Martinsen (1996), Shoreline trajectories and sequences: Description of variable depositional-dip scenarios, *J. Sediment. Res.*, *66*(4), 670–688.
- Hemming, S. R. (2004), Heinrich events: Massive late Pleistocene detritus layers of the North Atlantic and their global climate imprint, *Rev. Geophys.*, *42*, RG1005, doi:10.1029/2003RG000128.
- Hendriks, P. H. G. M. (2003), *In-Depth Gamma Ray Studies: Borehole Measurements*, Rijksuniversiteit Groningen, Holland.
- Hernandez-Molina, F. J., L. Somoza, J. Rey, and L. Pomar (1994), Late Pleistocene-Holocene sediments on the Spanish continental shelves: Model for very high resolution sequence stratigraphy, *Mar. Geol.*, *120*, 129–174, doi:10.1016/0025-3227(94)90057-4.
- Hiscott, R. N. (2001), Depositional sequences controlled by high rates of sediment supply, sea-level variations, and growth faulting: The Quaternary Baram Delta of northwestern Borneo, *Mar. Geol.*, *175*(1–4), 67–102, doi:10.1016/S0025-3227(01)00118-9.
- Hughen, K. A., et al. (2004), Marine04 Marine radiocarbon age calibration, 26 – 0 ka BP, *Radiocarbon*, *46*, 1059–1086.
- Hunt, D., and M. E. Tucker (1992), Stranded parasequences and the forced regressive wedge systems tract: Deposition during base-level fall, *Sediment. Geol.*, *81*, 1–9, doi:10.1016/0037-0738(92)90052-S.
- Jouet, G. (2007), Enregistrements stratigraphiques des cycles climatiques et glacio-eustatiques du Quaternaire terminal. Modelisation de la marge continentale du Golfe du Lion, 443 pp., Univ. de Bretagne Occidentale, Brest, France.
- Jouet, G., S. Berné, M. Rabineau, M. A. Bassetti, P. Bernier, and B. Dennielou (2006), Shoreface migrations at the shelf edge and sea-level changes around the Last Glacial Maximum (Gulf of Lions, NW Mediterranean Sea), *Mar. Geol.*, *234*(1–4), 21–42, doi:10.1016/j.margeo.2006.09.012.
- Lafuerza, S., J. Frigola, G. Jouet, M. A. Bassetti, N. Sultan, and S. Berne (2008), Subsea-floor stratigraphic profiling and soil classification from piezocone tests: A case study in the Gulf of Lion (NW Mediterranean Sea), *Geochem. Geophys. Geosyst.*, doi:10.1029/2007GC001845, in press.
- Leckie, D. A., and R. G. Walker (1982), Storm- and tide-dominated shorelines in Cretaceous Moosebar-Lower gates interval-outcrop equivalents of deep basin gas trap in western Canada, *Am. Assoc. Pet. Geol. Bull.*, *66*, 138–157.
- Lee, H. J., J. P. M. Syvitski, G. Parker, D. Orange, J. Locat, E. W. H. Hutton, and J. Imran (2002), Distinguishing sediment waves from slope failure deposits: Field examples, including the 'Humboldt slide', and modelling results, *Mar. Geol.*, *192*(1–3), 79–104, doi:10.1016/S0025-3227(02)00550-9.
- Lisiecki, L. E., and M. E. Raymo (2005), A Pliocene-Pleistocene stack of 57 globally distributed benthic $\delta^{18}O$ records, *Paleoceanography*, *20*, PA1003, doi:10.1029/2004PA001071.
- Lobo, F. J., J. M. Dias, F. J. Hernandez-Molina, R. Gonzalez, L. M. Fernandez-Salas, and V. Diaz Del Rio (2005), Late Quaternary shelf-margin wedges and upper slope progradation in the Gulf of Cadiz margin (SW Iberian Peninsula), *Geol. Soc. London Spec. Publ.*, *244*, 7–25, doi:10.1144/GSL.SP.2005.244.01.02.
- Lofi, J., et al. (2003), Plio-Quaternary prograding clinoform wedges of the western Gulf of Lion continental margin (NW Mediterranean) after the Messinian Salinity Crisis, *Mar. Geol.*, *198*(3–4), 289–317, doi:10.1016/S0025-3227(03)00120-8.
- Maillet, G. M., C. Vella, S. Berne, P. L. Friend, C. L. Amos, T. J. Fleury, and A. Normand (2006), Morphological changes and sedimentary processes induced by the December 2003 flood event at the present mouth of the Grand Rhone River (southern France), *Mar. Geol.*, *234*(1–4), 159–177, doi:10.1016/j.margeo.2006.09.025.
- Malatesta, A., and F. Zarlenga (1986), Northern guests in the Pleistocene Mediterranean Sea, *Geol. Romana*, *25*, 91–154.
- Martini, E. (1971), Standard Tertiary and Quaternary calcareous nannoplankton zonation, paper presented at 2nd Planktonic Conference 1970, Edizioni Tecnoscienza, Rome.
- Massari, F., M. Sgavetti, D. Rio, A. D'Alessandro, and G. Prosser (1999), Composite sedimentary record of falling stages of Pleistocene glacio-eustatic cycles in a shelf setting (Crotona basin, south Italy), *Sediment. Geol.*, *127*(1–2), 85–110, doi:10.1016/S0037-0738(99)00025-1.
- Mellere, D., and R. J. Steel (2000), Style contrast between forced regressive and lowstand/transgressive wedges in the Campanian of south-central Wyoming (Hatfield Member of the Haystack Mountains Formation), in *Sedimentary Responses to Forced Regressions*, edited by D. Hunt and R. Gawthorpe, *Geol. Soc. London Spec. Publ.*, *172*, 141–162.



- Monaco, A. (1971), Contribution à l'étude géologique et sédimentologique du plateau continental du Roussillon, doctoral thesis, 295 pp, Univ. of Perpignan, Perpignan, France.
- Pattison, S. A. J., and R. G. Walker (1995), Sequence stratigraphic significance of sharp-based lowstand shoreface deposits, Kenilworth Member, Book Cliffs, Utah, *J. Sediment. Petrol.*, 79(3), 444–462.
- Plint, A. G. (1988), Sharp-based shoreface sequences and “off-shore bars” in the Cardium Formation of Alberta: Their relationship to relative changes in sea level, in *Sea-Level Changes: An Integrated Approach, Spec. Publ.*, vol. 42, edited by C. K. Wilgus et al., pp. 357–370, Soc. for Sediment. Geol., Tulsa, Okla.
- Plint, A. G., and D. Nummedal (2000), The falling stage systems tract: Recognition and importance in sequence stratigraphy, in *Sedimentary Responses to Forced Regressions*, edited by D. Hunt and R. L. Gawthorpe, pp. 1–17, Geol. Soc., London.
- Posamentier, H. W., and G. P. Allen (1993), Variability of the sequence stratigraphic model: Effects of local basin factors, *Sediment. Geol.*, 86, 91–109, doi:10.1016/0037-0738(93)90135-R.
- Posamentier, H. W., G. P. Allen, D. P. James, and M. Tesson (1992), Forced regressions in a sequence stratigraphic framework: Concepts, examples and exploration significance, *Am. Assoc. Pet. Geol. Bull.*, 76, 1687–1709.
- Rabineau, M. (2001), Un modèle géométrique et stratigraphique des séquences de dépôt quaternaires sur la marge du Golfe du Lion: Enregistrement des cycles climatiques de 100,000 ans, Ph.D. thesis, 480 pp, Univ. of Rennes 1, Rennes, France.
- Rabineau, M., S. Berne, D. Aslanian, J.-L. Olivet, P. Joseph, F. Guillocheau, J.-F. Bourillet, E. Ledrezen, and D. Granjeon (2005), Sedimentary sequences in the Gulf of Lion: A record of 100,000 years climatic cycles, *Mar. Pet. Geol.*, 22(6–7), 775–804, doi:10.1016/j.marpetgeo.2005.03.010.
- Rabineau, M., S. Berne, J.-L. Olivet, D. Aslanian, F. Guillocheau, and P. Joseph (2006), Paleo sea levels reconsidered from direct observation of paleoshoreline position during Glacial Maxima (for the last 500,000 yr), *Earth Planet. Sci. Lett.*, 252(1–2), 119–137, doi:10.1016/j.epsl.2006.09.033.
- Raffi, I., and J. A. Flores (1995), Pleistocene through Miocene calcareous nannofossils from eastern equatorial Pacific Ocean (Leg 138), *Proc. Ocean Drill. Program Sci. Results*, 138, 233–286.
- Ramsey, N. (2002), A calibrated model for the interpretation of cone penetration tests (CPTs) in North Sea quaternary soils, in *Offshore Site Investigation and Geotechnics: Diversity and Sustainability*, edited by M. Cook et al., pp. 341–356, Soc. for Underwater Technol., London.
- Reimer, P. J., et al. (2004), IntCal04 Terrestrial radiocarbon age calibration, *Radiocarbon*, 46, 1029–1058.
- Ridente, D., F. Trincardi, A. Piva, A. Asioli, and A. Cattaneo (2008), Sedimentary response to climate and sea level changes during the past (400 kyr from borehole PRAD1-2 (Adriatic margin), *Geochem. Geophys. Geosyst.*, 9, Q09R04, doi:10.1029/2007GC001783.
- Robertson, P. K. (1990), Soil classification using the cone penetration test, *Can. Geotech. J.*, 27(1), 151–158, doi:10.1139/t90-014.
- Siddall, M., E. J. Rohling, A. Almogi-Labin, C. Hemleben, D. Meischner, I. Schmelzer, and D. A. Smeed (2003), Sea-level fluctuations during the last glacial cycle, *Nature*, 423, 853–858, doi:10.1038/nature01690.
- Storms, J. E. A., and G. J. Hampson (2005), Mechanisms for forming discontinuity surfaces within shoreface-shelf parasequences: Sea level, sediment supply, or wave regime?, *J. Sediment. Res.*, 75(1), 67–81.
- Stuiver, M., and P. J. Reimer (1993), Extended 14C database and revised CALIB radiocarbon calibration program, *Radiocarbon*, 35, 215–230.
- Surlyk, F., and N. Noe-Nygaard (2005), A forced-regressive shelf-margin wedge formed by transition-slope progradation: Lowermost Cretaceous Rauk Plateau Member, Jameson Land, East Greenland, *Bull. Geol. Soc. Den.*, 52, 227–243.
- Suter, J. R., and H. L. J. Berryhill (1985), Late Quaternary shelf-margin deltas, Northwest Gulf of Mexico, *Bull. Am. Assoc. Petrol. Geol.*, 69(1), 77–91.
- Sydow, J., H. H. Roberts, A. H. Bouma, and R. Winn (1992), Constructional subcomponents of a shelf-edge delta, North-east Gulf of Mexico, paper presented at the 42nd Annual Convention, Gulf Coast Assoc. of Geol. Soc., Jackson, Miss.
- Tamura, T., F. Nanayama, Y. Saito, F. Murakami, R. E. I. Nakashima, and K. Watanabe (2007), Intra-shoreface erosion in response to rapid sea-level fall: Depositional record of a tectonically uplifted strand plain, Pacific coast of Japan, *Sedimentology*, 54(5), 1149–1162, doi:10.1111/j.1365-3091.2007.00876.x.
- Tesson, M., B. Gensous, G. P. Allen, and C. Ravenne (1990), Late Quaternary lowstand wedges on the Rhône Continental Shelf, France, *Mar. Geol.*, 91, 325–332, doi:10.1016/0025-3227(90)90053-M.
- Tesson, M., et al. (1993), Late Pleistocene shelf-perched lowstand wedges on the Rhone continental shelf, in *Sequence Stratigraphy and Facies Associations, IAS Spec. Publ.*, vol. 18, edited by H. W. Posamentier et al., pp. 183–196, Blackwell Sci., Oxford, U. K.
- Tesson, M., H. W. Posamentier, and B. Gensous (2000), Stratigraphic organization of Late Pleistocene deposits of the western part of the Rhone shelf (Languedoc shelf) from high resolution seismic and core data, *AAPG Bull.*, 84(1), 119–150.
- Thierstein, H. R., K. R. Geitznauer, B. Molfino, and N. J. Shackleton (1977), Global synchronicity of late Quaternary coccolith datum levels: Validation by oxygen isotopes, *Geology*, 5, 400–404, doi:10.1130/0091-7613(1977)5<400:GSOLQC>2.0.CO;2.
- Trincardi, F., and A. Correggiari (2000), Quaternary forced regression deposits in the Adriatic Basin and the record of composite sea-level cycles, in *Sedimentary Responses to Forced Regressions*, edited by D. Hunt and R. L. Gawthorpe, pp. 245–269, Geol. Soc., London.
- Trincardi, F., and M. Field (1991), Geometry, lateral variability and preservation of downlapped regressive shelf deposits: Eastern Tyrrhenian margin, *Italy, J. Sediment. Petrol.*, 61, 775–790.
- van Wagoner, J. C., R. M. Mitchum, K. M. Campion, and V. D. Rahmanian (1990), *Siliciclastic Sequence Stratigraphy in Well Logs, Cores and Outcrops, Methods in Explor. Ser.*, vol. 7, 55 pp., Am. Assoc. of Petrol. Geol., Tulsa, Okla.
- Villanueva, J., J. A. Flores, and J. O. Grimalt (2002), A detailed comparison of the Uk'37 and coccolith records over the past 290 kyears: Implications to the alkenone paleotemperature method, *Org. Geochem.*, 33(8), 897–905, doi:10.1016/S0146-6380(02)00067-0.
- Walker, R. G., and A. G. Plint (1992), Wave- and storm-dominated shallow marine systems, in *Facies Models -*



Response to Sea Level Changes, edited by R. G. Walker and N. P. James, pp. 219–238, Geol. Assoc. of Can., St John's, Newfoundland, Canada.

Winn, R. D., H. H. Roberts, B. Kohl, R. H. Fillon, A. Bouma, and R. E. Constans (1995), Latest Quaternary deposition on the outer shelf, northern Gulf of Mexico: Facies and sequence stratigraphy from Main Pass Block 303 shallow core,

Geol. Soc. Am. Bull., 107(7), 851–866, doi:10.1130/0016-7606(1995)107<0851:LQDOTO>2.3.CO;2.

Winn, R. D., H. H. Roberts, B. Kohl, R. H. Fillo, J. A. Crux, A. H. Bouma, and H. W. Spero (1998), Upper Quaternary strata of the upper continental slope, northeast Gulf of Mexico: Sequence stratigraphic model for a terrigenous shelf edge, *J. Sediment. Res.*, 68(4), 579–595.